Involvements of Furry in YAP inactivation and 14-3-3 proteins in CEP97 degradation

博士論文

Involvements of Furry in YAP inactivation and 14-3-3 proteins in CEP97 degradation

(YAP 不活性化における Furry の役割と CEP97 分解における 14-3-3 の関与)

令和元年度

東北大学大学院生命科学研究科

分子生命科学専攻

入江　和樹

Table of contents

Abbreviations …… 2

Preface …… 3

(Chapter I)

Involvements of Furry in YAP inactivation

Abstract …… 6

Introduction …… 7

Results …… 9

Discussion ……. 13

Materials and methods ……. 15

References ……. 19

Figure Legends ……. 22

Figures ……. 25

(Chapter II)

Involvements of 14-3-3 proteins in CEP97 degradation

Abstract ……. 31

Introduction ……. 32

Results ……. 34

Discussion ……. 38

Materials and methods ……. 40

References ……. 43

Figure Legends ……. 45

Figures ……. 47

Acknowledgements ……. 54

Abbreviations

DAPI: 4',6-diamidino-2- phenylindole
DMEM: Dulbecco's modified Eagle's medium
DTT: dithiothreitol
FBS: fetal bovine serum
FOP: FGFR1OP
FRY: Furry
GFP: green fluorescent protein
GST: glutathione S-transferase
HEK: human embryonic kidney
HRP: horseradish peroxidase
IFT: intraflagellar transport
IB: immunoblot
IP: immunoprecipitation
IPTG: isopropyl b-D-thiogalactopyranoside
JBTS: Joubert syndrome
KO: knockout
LATS: large tumor suppressor
MCS: mammary caricinoma susceptibility
MDCK: Madin-Darby canine kidney
MKS: Meckel syndrome
MOB: Mps one binder
MST kinase: mammalian STE20-like kinase
NDR kinase: nuclear Dbf2-related kinase
NPHP: nephronophthisis
OA: okadaic acid
PBS: phosphate-buffered saline
PC: parental cell
PFA: paraformaldehyde
PVDF: polyvinylidene difluoride
RPE1: the telomerase-immortalized retinal pigment epithelial cell line
SD: standard deviation
S.E.M: standard error of the mean
PAGE: polyacrylamide gel electrophoresis
TAZ: transcriptional co-activator PDZ-binding motif
TBS: Tris-buffered saline
TEAD: TEA domain transcription factor
Trc: tricornered
TTBK2: tau-tubulin kinase 2
TUBEs: Tandem-repeated ubiquitin-binding entities
WT: wild type
YAP: Yes-associated protein

Preface

Cell-cell communication is critical for making multicellular organisms and maintaining their biological functions and homeostasis. Cell-cell communication is regulated by the signal transmission from signal-producing cells to signal-receiving cells. In response to extracellular signals, the signal-receiving cells change their states by intracellular signaling pathways. For example, growth factors interact their receptors present in cell surface and trigger the modulation of gene expression for cell proliferation; adhesion receptors transmit the mechanical and chemical signals from the neighboring cells and extracellular matrix. The complexity of cell-cell communication has been investigated for long decades, but further studies are required for elucidating the molecular mechanisms of cell-cell communication and intracellular signaling systems. In this thesis, I investigated the mechanisms of two signaling processes, the Hippo pathway and the growth-arrest-induced ciliogenesis".

The organ size in multicellular organisms is well controlled by the balance of cell proliferation, apoptosis, stem cell self-renewal and differentiation. Intracellular and extracellular factors tightly regulate these processes, which are essential for normal embryonic development, organogenesis and tissue homeostasis. The aberrations of these regulation systems cause developmental disorder, tumorigenesis and several human diseases.

The Hippo pathway has been established as a signaling pathway that restricts cell proliferation and organ size. This pathway was firstly identified in *Drosophila*, and the components of this pathway are evolutionarily conserved from yeast to human. The core components of this pathway in mammalian cells are MST1/2 kinases, SAV, LATS1/2 kinases YAP and TAZ. When the cells sense the growth arrest signals, MST1/2 kinases bind to their adaptor protein SAV and phosphorylate and activate downstream kinases, NDR1/2 and LATS1/2. LATS1/2 kinases directly interact with and phosphorylate transcriptional co-activators, YAP and TAZ, to promote their cytoplasmic retention or degradation, resulting in the inhibition of their interactions with TEAD and TEAD-mediated transcriptional activation and thereby the suppression of cell proliferation. Whereas the crucial role of LATS1/2 kinases in YAP inactivation is well known, several studies have shown that LATS1/2 are occasionally dispensable for YAP phosphorylation and inactivation, suggesting that other protein kinase(s) is involved in YAP inactivation. A recent study demonstrated that NDR1/2 also phosphorylate and inactivate YAP. However, the mechanisms regulating YAP phosphorylation is not fully understood.

In chapter I of this thesis, I provide evidence that FRY, a novel YAP-binding protein, is crucial for the regulation of YAP localization and phosphorylation. I also demonstrate that FRY promotes the cytoplasmic sequestration of YAP by two mechanisms, increasing the kinase activity of NDR1/2 and associating with YAP.

Primary cilia are antenna-like structures that protrude from the cell surface and are present in most vertebrate cell types. Numerous ion channels and receptors for various signaling are enriched in primary cilia. Primary cilia are essential for development, such as the formation of brain and limb. The defects in the formation and function of cilia result in serious developmental disorders, called ciliopathies.

Primary cilia consist of microtubule-based axoneme, transition-zone, and basal body derived from the mother centriole. Uponr the growth arrest signaling, primary cilia assemble through series of rapid and well-orchestrated events. CP110 and CEP97 proteins are the key negative-regulators for cilia formation. The CP110 and CEP97 complex normally forms a cap at the distal end of the centrioles to prevent microtubule growth in proliferating cells. Upon serum starvation, the CP110-CEP97 complex is specifically released from the mother centriole. A recent study in my laboratory showed that CEP97 is degraded upon serum starvation by the ubiquitin-proteasome system. This study identified the CUL3-RBX1-KCTD10 complex as the E3 ubiquitin ligase complex required for CEP97 ubiquitination and degradation in quiescent cells. However, the mechanism of CEP97 degradation upon serum starvation remains to be solved.

In chapter II of this thesis, I analyzed the KCTD10-binding proteins that are involved in CEP97 ubiquitination during the cilium formation. I show that 14-3-3 proteins interact with KCTD10 and CEP97 and provide evidence that 14-3-3 proteins are involved in CEP97 ubiquitination and its removal from the mother centriole during ciliogenesis.

Chapter I

Involvements of Furry in YAP inactivation

Abstract

The Hippo signaling pathway negatively regulates cell proliferation and tumorigenesis. In the canonical Hippo pathway, LATS1/2 kinases phosphorylate the transcriptional coactivator YAP and thereby suppress its nuclear localization and co-transcriptional activity. A recent study showed that NDR1/2, the kinases closely related to LATS1/2, also phosphorylate and inactivate YAP by suppressing its nuclear localization. Furry (FRY) is a cytoplasmic protein that associates with NDR1/2 and activates their kinase activities, but its role in the nuclear/cytoplasmic localization of YAP remains unknown. In this study, I constructed FRY knockout cell lines and examined the role of FRY in YAP localization. Depletion of FRY markedly promoted YAP nuclear localization. FRY depletion decreased the kinase activity of NDR1/2 and the levels of YAP phosphorylation, but did not affect LATS1/2 kinase activity. This indicated that FRY suppressed YAP nuclear localization by promoting YAP phosphorylation via activation of NDR1/2. Depletion of NDR1/2 also promoted YAP nuclear localization, but depletion of both FRY and NDR1/2 more prominently increased the number of cells with YAP nuclear localization compared with depletion of NDR1/2 alone, suggesting that FRY suppressed YAP nuclear localization by a mechanism in addition to NDR1/2 activation. Co-precipitation assays revealed that FRY bound to YAP through the N-terminal region. Expression of full-length FRY or its 1-2400 N-terminal fragment restored YAP cytoplasmic localization in FRY-knockout cells. Taken together, these results suggest that FRY plays a crucial role in YAP cytoplasmic retention via NDR1/2 kinase activation and by binding to YAP, leading to its cytoplasmic sequestration.

Introduction

The Hippo signaling pathway plays a key role in controlling organ size control, tissue homeostasis, and tumorigenesis by regulating cell proliferation and survival (1–3). This pathway was originally identified in Drosophila with the major components of the pathway being evolutionarily conserved in mammals (1–3). The core components of the canonical Hippo pathway in mammalian cells are a kinase cascade, composed of mammalian STE20-like kinase 1 and 2 (MST1 and MST2), which are orthologs of Drosophila Hippo, large tumor suppressor 1 and 2 (LATS1 and LATS2), which are orthologs of Drosophila Warts, and the transcriptional coactivators Yes-associated protein (YAP) and transcriptional coactivator with PDZ-binding motif (TAZ), which are orthologs of Drosophila Yorkie. MST1/2 kinases phosphorylate and activate LATS1/2 kinases, which in turn phosphorylate YAP/TAZ, resulting in its cytoplasmic sequestration by 14-3-3 proteins or its proteasomal degradation, thereby inhibiting their co-transcriptional activity for cell proliferation and survival (1–3). When the Hippo pathway is inactivated, YAP/TAZ preferentially localize to the nucleus and promote cell proliferation by stimulating transcription factors, such as the TEA domain transcription factor (TEAD), which is an ortholog of Drosophila Scalloped (2, 3). Overexpression or hyperactivation of YAP often results in organ overgrowth and tumor development, thus the precise control of the nuclear/cytoplasmic localization and activity of YAP is important for tissue homeostasis and tumor suppression (4, 5).

The Hippo pathway and its effector YAP are regulated by a wide range of molecules that have roles in cell-cell and cell-substrate adhesions, cell morphology, and cell polarity (3, 6–8). Mechanical stresses and changes in actin cytoskeletal dynamics also affect the nuclear/cytoplasmic localization of YAP (9–11). Whereas the crucial role of LATS1/2 kinases in YAP regulation is well known, several studies have shown that LATS1/2 are occasionally dispensable for YAP phosphorylation and inactivation (11–15), suggesting that other protein kinase(s) may be involved in YAP regulation. Nuclear Dbf2-related (NDR) kinases, consisting of NDR1 and NDR2 in mammals, are the closest homologs of LATS1/2 in the AGC family of serine/threonine kinases (16, 17). A recent study demonstrated that NDR1/2 kinases also phosphorylate YAP and inhibit its nuclear localization (18). The loss of NDR1/2 in the murine intestinal epithelium causes decreased YAP phosphorylation and promotes chemically induced colon carcinogenesis (18), indicating that NDR1/2 kinases serve as tumor suppressors by phosphorylating YAP and inhibiting its nuclear localization.

The kinase activity of NDR is regulated by several mechanisms, including the binding of MOB proteins to the N-terminal MOB-binding domain, trans-phosphorylation of the C-terminal hydrophobic motif by upstream MST kinases, and auto-phosphorylation of the activation segment in the kinase catalytic domain (16). NDR is also activated by Furry (FRY) (19–21), although little is known regarding the molecular mechanism of FRY activating NDR kinase activity.

FRY is an evolutionarily conserved large cytoplasmic protein in eukaryotes (22). In model organisms, FRY orthologs genetically and physically interact with NDR orthologs (19–22). For instance, FRY and NDR orthologs cooperatively function to control polarized cell growth and morphogenesis in yeast, neurite outgrowth in nematodes, and epidermal morphogenesis and dendritic tiling in fruit flies (19, 20, 22–26). In mammalian cells, I previously showed that FRY physically associates with NDR1 and activates its kinase activity and that FRY, through NDR1 activation, is crucial for mitotic chromosome alignment in cultured cells (21). Since NDR1/2 kinases are shown to be involved in the cytoplasmic sequestration of YAP (18), I hypothesized that FRY plays a role in the nuclear/cytoplasmic localization of YAP.

In the current study, I constructed FRY knockout cell lines and examined the role of FRY in the nuclear/cytoplasmic localization of YAP. I show that the depletion of FRY significantly promotes YAP nuclear localization and that the expression of FRY restores YAP cytoplasmic localization in FRY-knockout cells. I also provide evidence that

FRY promotes the cytoplasmic sequestration of YAP by increasing the kinase activity of NDR1/2 and by associating with YAP.

Results

FRY depletion promotes nuclear localization of YAP and TAZ

Previous studies using cells cultured under serum-supplemented conditions have shown that at low cell density YAP predominantly localizes to the nucleus, but at high cell density it primarily localizes to the cytoplasm (9, 15, 27). To examine whether FRY is involved in the nuclear/cytoplasmic localization of YAP, I generated FRY-knockout (FRY-KO) HEK293A cell lines using the CRISPR/Cas9 system and analyzed the effects of FRY depletion on YAP nuclear/cytoplasmic localization. Immunoblot analyses revealed that FRY protein was depleted in each of two independently-generated FRY-KO cell lines (Fig. 1A). The parental HEK293A cells and the two FRY-KO cell lines were cultured at low (1.6×10^4 cells/cm^2) and high (8.0×10^4 cells/cm^2) cell densities in medium containing 10% serum and YAP localization was analyzed by immunostaining with an anti-YAP antibody. The nuclei were stained with 4',6-diamidino-2-phenylindole (DAPI).

As previously reported for other cells (9, 15, 27), YAP almost completely localized to the nucleus at low cell density but localized preferentially to the cytoplasm at high cell density in the parental HEK293A cells (Fig. 1B). In contrast, whereas the predominant localization of YAP in the nucleus was not affected by FRY depletion in cells cultured at low density, YAP preferentially localized to the nucleus in the two FRY-KO cell lines cultured at high density (Fig. 1B). Quantitative analyses showed that under conditions of high cell density, FRY depletion significantly increased the percentage of cells with nuclear YAP localization (Fig. 1C). More than 70% of the FRY-KO cells exhibited YAP localization in the nucleus, whereas only 23% of the parental cells exhibited YAP localization in the nucleus. These results suggest that FRY is involved in the cytoplasmic sequestration of YAP in cells cultured at high density.

The nuclear/cytoplasmic localization of YAP was further examined by subcellular fractionation analysis. The lysates of the parental and FRY-KO cells were fractionated into the nuclear and cytoplasmic fractions and analyzed by immunoblotting with an anti-YAP antibody, YAP was mostly detected in the nuclear fraction in both of the parental and FRY-KO cells cultured at low density (Fig. 1D). In contrast, at high density, YAP was predominantly detected in the cytoplasmic fraction in parental cells but it was detected in both the nuclear and cytoplasmic fractions in FRY-KO cells(Fig. 1D). These results further support the role of FRY in the cytoplasmic retention of YAP at high cell density.

I also examined the effect of FRY knockout on the nuclear/cytoplasmic localization of TAZ, a paralogue of YAP. Similar to the effect on YAP localization, knockout of FRY significantly increased the population of cells with nuclear localized TAZ at high cell density (Fig. 1E, F).

I also analyzed the effect of FRY knockout on the co-transcriptional activity of YAP/TAZ by luciferase reporter assays using a YAP/TAZ-responsive reporter (8xGTIIC-luciferase), which contains eight TEAD-binding sites (11, 13). The reporter assays revealed that depletion of FRY increased the YAP/TAZ reporter activity (Fig. 1G).

FRY depletion decreases NDR1/2 kinase activities and YAP phosphorylation levels

A previous study using intestinal epithelial cells demonstrated that NDR1/2 kinases promote the cytoplasmic localization of YAP via its phosphorylation at Ser-127 (18). Since FRY genetically and physically interacts with NDR kinases and promotes their kinase activities (22), I hypothesized that FRY is involved in the cytoplasmic localization of YAP by promoting NDR1/2 kinase activities and YAP phosphorylation. To address this possibility, I examined the effects of FRY depletion on the kinase activities of NDR1 and NDR2 and the level of YAP phosphorylation. To measure NDR1 and NDR2 kinase activity, lysates of the parental and FRY-KO HEK293A cells were immunoprecipitated with an anti-

NDR1 or an anti-NDR2 antibody and the precipitates were subjected to *in vitro* kinase assays, using glutathione S-transferase (GST)-YAP as a substrate. The YAP phosphorylating activities of NDR1 and NDR2 were suppressed in the FRY-KO cells, compared to those in the parental cells (Fig. 2A). I also examined the effects of FRY knockout on the level of the kinase activities of LATS1 and LATS2. In contrast to the effects of NDR1/2, FRY depletion had no apparent effect on the kinase activities of LATS1 and LATS2 (Fig. 2B), suggesting a specific role for FRY in NDR1/2 kinase activation.

I next examined the effect of FRY knockout on the level of YAP phosphorylation in the cells. Lysates of the parental and FRY-KO cells were analyzed by immunoblotting with an anti-YAP antibody and an anti-phospho-Ser-127-YAP (pS127-YAP) antibody that specifically recognizes the Ser-127-phosphorylated form of YAP. The level of YAP phosphorylation was decreased in the FRY-KO cells, compared to that in the parental cells (Fig. 2C). Quantitative analysis showed that the level of YAP phosphorylation, as measured by the ratio of pS127-YAP to total YAP, was significantly decreased in the FRY-KO cells (Fig. 2D). These results suggest that FRY depletion promotes the nuclear localization of YAP, at least in part by decreasing NDR1 and NDR2 kinase activities, which leads to reduced levels of YAP phosphorylation.

Knockdown of NDR1/2 kinases decreases YAP phosphorylation

To examine the role of NDR kinases in the cytoplasmic localization of YAP, I analyzed the effects of NDR1/2 double knockdown on the levels of YAP phosphorylation and on YAP nuclear/cytoplasmic localization. HEK293A cells were treated with a mixture of NDR1- and NDR2-targeting small interfering RNAs (NDR1/2 siRNAs). Immunoblot analyses revealed that treatments of HEK293A cells with NDR1/2 siRNAs suppressed the levels of both NDR1 and NDR2 proteins (Fig. 3A). Immunoblot analysis of lysates from HEK293A cells treated with NDR1/2 siRNAs with anti-pS127-YAP and anti-YAP antibodies revealed that the level of YAP phosphorylation was significantly decreased in NDR1/2 double knockdown cells, compared to that in control cells (Fig. 3B, C). This indicates that NDR1/2 kinases are involved, at least in part, in YAP phosphorylation in HEK293A cells. The degree of the decrease in YAP phosphorylation in the NDR1/2-double-knockdown cells was similar to that in the FRY-KO cells, suggesting that FRY depletion decreases the level of YAP phosphorylation through NDR1/2 inactivation.

Effects of NDR1/2 knockdown on YAP nuclear localization in parental and FRY-KO cells

I then analyzed the effects of NDR1/2 double knockdown on the nuclear/cytoplasmic localization of YAP in HEK293 parental cells and FRY-KO cells. In the parental cells, double knockdown of NDR1/2 increased the number of cells with nuclear localized YAP, indicating that NDR1/2 kinases are involved in the cytoplasmic localization of YAP (Fig. 3D, E). In contrast, double knockdown of NDR1/2 in FRY-KO cells had no significant effect on the number of the cells with nuclear localized YAP (Fig. 3D, E). These results support the notion that FRY depletion causes the nuclear localization of YAP through NDR1/2 inactivation. Intriguingly, the proportion of the cells with nuclear YAP localization in NDR1/2 siRNA-treated FRY-KO cells was higher than that in NDR1/2 siRNA- treated parental cells (Fig. 3D, E). These results suggest that FRY is involved in the cytoplasmic localization of YAP by a mechanism(s) in addition to the activation of NDR1/2 kinases.

Effects of LATS1/2 knockdown on YAP phosphorylation and YAP nuclear localization

I also examined the effects of LATS1/2 knockdown on the levels of YAP phosphorylation and on YAP nuclear/cytoplasmic localization. The level of YAP phosphorylation was markedly decreased by LATS1/2 double

knockdown in both parental and FRY-KO cells (Fig. 3F). The residual pS127-YAP in the FRY-KO cells was further decreased by LATS1/2 double knockdown (Fig. 3F), indicating that LATS1/2 kinases are involved in YAP phosphorylation in HEK293A cells, independently of FRY. Immunostaining showed that double knockdown of LATS1/2 increased the population of the cells with nuclear localized YAP in both parental and FRY-KO cells, and the effects of FRY knockout and LATS1/2 knockdown on YAP nuclear localization were additive (Fig. 3G, H). These results suggest that LATS1/2 kinases play crucial role in YAP phosphorylation and its cytoplasmic localization, but its action is independent of FRY.

YAP binds to FRY

To investigate the additional mechanism, by which FRY promotes the cytoplasmic localization of YAP, I examined the possibility that FRY binds to YAP leading to it being sequestered in the cytoplasm. I analyzed the YAP-binding ability of FRY using co-immunoprecipitation assays. When green fluorescent protein (GFP)-tagged YAP and (Myc+His)-tagged FRY were co- expressed in HEK293T cells and the cell lysates were immunoprecipitated with an anti-GFP antibody, FRY-(Myc+His) was co-precipitated with GFP-YAP (Fig. 4A). I also analyzed the interaction between endogenous FRY and YAP using co-precipitation assays. HEK293A cell lysates were immunoprecipitated with an anti-FRY antibody and the precipitates were analyzed by immunoblotting with anti-FRY and anti-YAP antibodies. Endogenous YAP was co-precipitated with the endogenous FRY (Fig. 4B). These results indicate that FRY binds to YAP in cells.

I then constructed the N- and C-terminal fragments of FRY, FRY-N-(1-2400) and FRY-C- (1550-3020), respectively (Fig. 4C) and analyzed their abilities to bind YAP. GFP-YAP and (Myc+His)-tagged FRY fragments were co- expressed in HEK293T cells and the cell lysates were immunoprecipitated with an anti-GFP antibody. Blotting results revealed that FRY-N-(1- 2400), but not FRY-C-(1550-3020), was co-precipitated with GFP-YAP (Fig. 4D). This indicates that FRY binds to YAP through its N-terminal (1-2400) region. To further define the YAP-binding region of FRY, I constructed two additional FRY fragments, N-(1-730) and M-(718-1575) (Fig. 4C) and analyzed their YAP-binding abilities. Co-precipitation assays revealed that FRY-M-(718-1575), but not FRY-N-(1-730), was bound to YAP (Fig. 4E).

The cytoplasmic localization of YAP is promoted by phosphorylation and subsequent binding of 14-3-3 proteins, which sequester YAP in the cytoplasm. To determine whether the interaction between YAP and FRY is affected by YAP phosphorylation, I constructed YAP-5SA, a non-phosphorylatable mutant in which all five serine residues (S61, S109, S127, S164, and S394) matching the LATS/NDR target consensus motif (HXRXXS) were replaced by alanine (28). YAP-5SA was then analyzed for its ability to bind to FRY. When GFP-tagged wild-type (WT) YAP and its 5SA mutant were co-expressed with (Myc+His)-tagged FRY in HEK293T cells and immunoprecipitated with an anti-GFP antibody, similar amounts of FRY-(Myc+His) were co- precipitated with GFP-YAP-WT and GFP-YAP-5SA (Fig. 4F). This indicates that in contrast to 14-3-3 proteins, FRY binds to YAP, irrespectively of the phosphorylation state of YAP. Taken together, these results suggest that FRY has the potential to bind to YAP and thereby promotes its cytoplasmic retention.

Expression of FRY or its N-terminal (1-2400) fragment restores YAP cytoplasmic localization in FRY- knockout cells

I performed knockout/rescue experiments to confirm the functional role of FRY in the cytoplasmic localization of YAP, as well as to examine the correlation between YAP cytoplasmic localization and the YAP-binding ability of FRY. FRY-KO cells were transfected with expression plasmids encoding control GFP, (Myc+His)-tagged FRY, or its N- or C-terminal fragments. The transfected cells were cultured at a high cell density, fixed, and then stained with an anti-YAP

antibody (Fig. 5A). Expression of GFP and (Myc+His)-tagged FRY were visualized with GFP fluorescence imaging and anti-Myc immunostaining, respectively. The cell nuclei were stained with DAPI. The effects of the expression of these proteins on YAP localization were analyzed by determining the percentage of the cells with nuclear localized YAP in GFP- or Myc-positive cells. The proportion of cells with nuclear localized YAP was significantly greater in FRY-KO cells transfected with control GFP than that in parental cells transfected with GFP (Fig. 5A, B). Compared with that in the GFP transfection controls, transfection of FRY-KO cells with full-length FRY or FRY-N-(1-2400) resulted in a significantly lower percentage of cells with nuclear localized YAP, similar to the level observed in GFP-transfected parental cells (Fig. 5A, B). In contrast, transfection of FRY-KO cells with FRY-C-(1550-3020) did not affect the nuclear localization of YAP (Fig. 5A, B). These results suggest that the N-terminal (1-2400) region of FRY is crucial for its function in promoting YAP cytoplasmic localization.

I also examined the effects of expression of FRY fragments, N-(1-730) and M-(718-1575), on YAP nuclear localization in FRY-KO cells. Knockout/rescue experiments showed that these two fragments had no apparent effect on the nuclear localization of YAP in FRY-KO cells (Fig. 5C, D). FRY-M-(718-1575) has the potential to bind to YAP, but did not rescue the suppressive effect of FRY knockout on YAP cytoplasmic localization, indicating that the YAP-binding ability alone is not sufficient for FRY to promote YAP localization to the cytoplasm.

Discussion

In this study, I showed that FRY depletion markedly induces nuclear localization of YAP, indicating that FRY plays a crucial role in sequestering YAP in the cytoplasm. Consistent with earlier studies showing that FRY activates NDR kinases and that NDR kinases phosphorylate YAP (18, 21), depletion of FRY resulted in decreased NDR1/2 kinase activities and decreased YAP phosphorylation. However, FRY depletion did not affect LATS1/2 kinase activities, indicating that FRY has a specific role in the activation of NDR1/2, but not in the activation of LATS1/2 and that FRY increases YAP phosphorylation through the activation of NDR1/2. Depletion of NDR1/2 also decreased YAP phosphorylation and promoted the nuclear localization of YAP. However, the extent of YAP nuclear localization in NDR1/2-depleted FRY- KO cells was significantly higher than that in NDR1/2-depleted parental cells, which suggests that FRY suppresses YAP nuclear localization through both NDR-dependent and NDR- independent mechanisms. With respect to this, I showed that FRY binds to YAP via the N- terminal (1-2400) region. Both full-length FRY and its N-terminal (1-2400) fragment restored YAP cytoplasmic localization in FRY-KO cells. This was in contrast to the C-terminal (1560- 3020) fragment of FRY, which did not exhibit YAP-binding ability and failed to restore YAP cytoplasmic localization. Taken together, these results suggest that FRY plays a crucial role in the cytoplasmic retention of YAP by two mechanisms, the enhancement of YAP phosphorylation through NDR1/2 kinase activation and the direct binding to YAP, which leads to YAP sequestration in the cytoplasm. NDR1/2-mediated YAP phosphorylation probably causes YAP sequestration in the cytoplasm by promoting its association with 14- 3-3 proteins (18, 27).

Further analysis of the YAP-binding region of FRY revealed that FRY-M-(718-1575), but not FRY-N-(1-730), binds to YAP. FRY-M-(718-1575) had the YAP-binding ability, but did not rescue the cytoplasmic localization of YAP in FRY-KO cells. This result indicates that the YAP-binding ability is not sufficient for FRY to exhibit its function to promote the cytoplasmic retention of YAP. Because It is likely that the M-(718-1575) fragment failed to activate NDR kinases, because FRY binds to NDR1 via its N-terminal (1-730) region (21). Moreover, this fragment appears to lose the ability of its own localization to the cytoplasm.

Previous studies have shown that NDR kinases are activated by several mechanisms, including the binding of MOB proteins to the N- terminal MOB-binding domain, the trans- phosphorylation of the C-terminal hydrophobic motif by upstream MST kinases, and the auto- phosphorylation of the activation segment in the kinase catalytic domain (16, 17). FRY is genetically linked to NDR kinases in most model organisms, including yeast, nematodes and fruit flies, suggesting a role of FRY being an activator of NDR kinases (22). Our group previously showed that in mammals, FRY binds to and promotes NDR1 kinase activity upon treatment with okadaic acid, an inhibitor of protein phosphatase PP2A (21). In the current study, I showed that the kinase activities of NDR1/2 decreased in FRY-KO cells, which further confirmed the role of endogenous FRY in NDR1/2 kinase activation. A recent crystallographic study demonstrated that an atypically long activation segment in the kinase domain of NDR1 covers the kinase catalytic surface and serves an auto-inhibitory role (29). That report also showed that the deletion of the activation segment and okadaic acid treatment enhanced the kinase activity of NDR1 and its association with FRY (29). These results suggest that the NDR1-binding and NDR1-activating abilities of FRY are enhanced by phosphorylation and the detachment of the auto-inhibitory segment from the kinase catalytic site. However, only little is actually known regarding the mechanism by which FRY regulates NDR kinase activity. Further studies are required to define the precise molecular mechanisms underlying FRY- mediated NDR kinase activation.

In mammalian cells, NDR1/2 kinases are involved in centrosome duplication, chromosome alignment, apoptosis, and proliferation (21, 30–32). While a crucial role of FRY in NDR1 kinase activation for the fidelity of mitotic

chromosomal alignment has been shown (21), it remains unknown whether FRY is involved in other cellular processes. It will be intriguing to explore whether FRY collaborates with NDR kinases to regulate these processes. A previous study showed that the ablation of NDR1 predisposes mice to the development of T cell lymphoma (31). In addition, another recent report showed that the conditional knockout of NDR1/2 in intestinal epithelia results in hyperplasia of colon epithelia and facilitates the development of chemically induced colon carcinoma (18). The latter report demonstrated that NDR1/2 kinases phosphorylate YAP and sequester it in the cytoplasm of cells in the intestinal epithelium. These results suggest that NDR kinases function as tumor suppressors by inhibiting the nuclear localization of YAP. Since FRY suppresses the nuclear localization of YAP through NDR1/2 kinase activation, it is conceivable that FRY also functions as a tumor suppressor by suppressing YAP nuclear localization. With respect of this, a recent report suggested that *Fry* is a candidate mammary carcinoma susceptibility gene in rats and showed that the levels of *Fry* mRNA and Fry protein are reduced in human breast cancer cell lines compared with those in non-tumorigenic cell lines (33). These results are consistent with the possibility that FRY has a tumor suppressive role. A quite recent report showed that ectopic expression of FRY suppresses the growth and proliferation in cancer cells (34). They showed that FRY is required for mammary gland development. It will be important to determine the effects of FRY knockout on tumorigenesis in model animals.

FRY and NDR orthologs (Sax-2 and Sax-1 in *C. elegans*, and Furry and Trc in *Drosophila*, respectively) cooperatively function in the dendritic branching and tiling (22, 24, 26). In human, the *Fry* gene has been identified as one of the candidate genes involved in intellectual disability (35),; however, the precise roles of FRY and NDR in the mammalian nervous system remains unknown. Furthermore, it remains unknown whether FRY and NDR orthologs in model organisms modulate neurite morphology and development by regulating YAP activity. Future studies using model animals will help us to better understand the roles of the FRY-NDR-YAP pathway in tumorigenesis and neural development.

Materials and Methods

Reagents and antibodies

Rabbit polyclonal antibodies against FRY, NDR1 and NDR2 were raised against their partial peptide sequences, TTFLPDSSVSGTSL, TARGAIPSYMKAAK, and SDILQPVPNTTEPDYKS, respectively, as previously reported (21, 36). Rabbit polyclonal antibodies against LATS1 (#9153, Cell Signaling Technology), LATS2 (GTX87529, Gene Tex), c- Myc (562; Medical and Biological Laboratories), and GFP (A6455, Molecular Probes) were purchased from the specified suppliers. Rabbit monoclonal antibodies against Ser-127- phosphorylated YAP (pS127-YAP) (#130008), and histone H3 antibody (#9715S), were purchased from Cell Signaling Technology. Mouse monoclonal antibodies against c-Myc (9E10, Roche), c-Myc (PL14, Medical and Biological Laboratories), YAP (sc-101199, Santa Cruz), TAZ (Cat:560235, BD Pharmingen) and α-tubulin (B-5-1-2, Sigma) were purchased from the specified suppliers. Secondary antibodies conjugated with horseradish peroxidase (HRP) against mouse IgG (NA931, GE Healthcare) and rabbit IgG (NA934, GE Healthcare) were purchased from the suppliers indicated. Secondary antibodies conjugated with Alexa Fluor 488 against mouse IgG (A11029) and rabbit IgG (A11034) and those with Alexa Fluor 568 against mouse IgG (A11031) were purchased from Life Technologies.

Plasmid construction

Complementary DNA (cDNA) coding for human YAP isoform 1 (NM_001130145.2) was PCR-amplified from a megaman human transcriptome library (Agilent). The cDNA was subcloned into GFPk and pGEX expression vectors (Invitrogen). The cDNA plasmid encoding YAP(5SA), in which five serine residues (S61, S109, S127, S164, and S397) were replaced with alanine (28), was constructed using a site-directional mutagenesis kit (Agilent). The cDNA for mouse FRY was PCR-amplified from mouse brain cDNA library and subcloned into a pcDNA3.1/Myc+His expression vector (Invitrogen), as described previously (21). The cDNA plasmids encoding FRY deletion mutants were constructed by PCR amplification, as previously reported (37).

Cell culture and transfection

HEK293T and HEK293A cells were cultured in Dulbecco's modified Eagle's medium (Wako Pure Chemical Industries) supplemented with 10% fetal bovine serum (FBS, Biosera). Transfections were performed using RNAi MAX (Invitrogen), Fugene HD (Promega), or jet PEI (Polyplus), according to manufactures' protocols. Cells were harvested at 40 h post-transfection for immunoblot analyses.

Gene knockout of HEK293A cells using the CRISPR/Cas9 system

The guide sequences were designed using the CRISPR design tool at https://crispr.dbcls.jp/ or the archived guide sequences from a genome- scale CRISPR knockout (GeCKO2) library (38). The sequences of guide RNAs used for human FRY knockout were as follows: #1, 5'-ACG CAA GAT TCG TAT CAT TA-3' and #2, 5'-CAC AGA ATT CAG TCG GAA CG-3'. The guide sequences were cloned into a Cas9 expression plasmid (PX459; Addgene plasmid no.62988). HEK293A cells were transfected with the Cas9 plasmids, selected with puromycin, and cloned by limited-dilution as described previously (39). Knockout clones were selected by immunoblot analyses using an anti-FRY antibody.

RNA interference

The Stealth siRNAs and silencer siRNAs were purchased from Thermo Fisher Sciences. The targeting sequences were as follows: siNDR1#1, 5'-GGC AGA CAG UUU GUG GGU UGU GAA A-3'; siNDR1#2, 5'-GCA AUG AAA AUA CUC CGU ATT-3'; siNDR2#1, 5'-GGC CAG CAG CAA UCC CUA UAG AAA U-3'; and siNDR2#2, 5'-GGU UUG AAG GGU UGA CUC ATT-3', siLATS1#1, 5'- CCU CCA UAC GAG UCA AUC ATT-3'; siLATS1#2, 5'-GGA GUG AUG AUA ACG AGG ATT-3'; siLATS2#1, 5'- GUU CGG ACC UUA UCA GAA ATT-3'; and siLATS2#2, 5'- GCA UUU UAC GAA UUC ACC UTT-3'.A mixture of siNDR1#1 and siNDR2#1 (siNDR1/2#1), siNDR1#2 and siNDR2#2 (siNDR1/2#2), siLATS1#1 and siLATS2#1, or siLATS1#2 and siLATS2#2 was used for double knockdown of NDR1 and NDR2, or LATS1 and LATS2. A Stealth RNAi negative control (Thermo Fisher Sciences) was used as the control siRNA.

Immunoprecipitation assay

For preparation of cell lysates, cells were washed once with phosphate-buffered saline (PBS) and lysed with lysis buffer (50 mM Tris- HCl (pH 7.5), 1% (v/v) Triton X-100, 150 mM NaCl, 5% (v/v) glycerol, 1 mM EGTA, 50 mM sodium fluoride, 1 mM sodium vanadate, 1 mM PMSF, 1 mM dithiothreitol (DTT), 10 μg/ml leupeptin, and 3 μg/ml pepstatin A). The lysates were cleared by centrifugation at 15,000 rpm for 10 min at 4°C. For the immunoprecipitation assays, cell lysates were pre-cleared with nProtein A Sepharose Fast Flow (GE Healthcare) and the supernatants were incubated with the indicated antibodies for 4 h at 4°C. After centrifugation, the beads were washed four times with wash buffer (500 mM NaCl, 50 mM Tris-HCl, 1% Triton X-100, 5% glycerol, and 1 mM DTT) and the precipitates were boiled in SDS sample buffer (62.5 mM Tris-HCl (pH 6.8), 2% SDS, 5% 2-mercaptoethanol, 5% sucrose, and 0.005% bromophenol blue) for 5 min at 97°C, subjected to SDS-PAGE, and analyzed by immunoblotting using the indicated antibodies.

Immunoblotting

Samples were separated by SDS-PAGE and transferred onto Immobilon-P polyvinylidene difluoride membranes (Millipore). The membranes were blocked with 5% non-fat dry milk in 0.05% Tween 20-containing PBS (PBS- T) or with Blocking One P (Nakalai Tesque) for 1 h. The membranes were incubated with the primary antibodies for 1.5 h at room temperature or overnight at 4°C. After washing the membranes three times with PBS-T or 0.05% Tween 20-containing Tris-buffered saline (TBS- T), they were incubated with HRP-conjugated secondary antibody for 1.5 h. After washing, the membranes were reacted with Immobilon Western (Millipore) and the immunoreactive protein bands were visualized using a LAS-4000 Bioimaging Analyzer (GE Healthcare) or ChemiDoc Touch Imaging System (Bio-Rad). Images were analyzed by using ImageJ.

Immunostaining and fluorescence microscopy

Cells were cultured at low density ($1.6 \times 10^4/cm^2$) or high density ($8.0 \times 10^4/cm^2$) for 24 hours. Cells were fixed with 4% paraformaldehyde at room temperature for 30 min, washed twice with PBS for 5 min, and then permeabilized by treatment with 0.1% Triton X-100 in PBS for 5 min at room temperature. After two washes with PBS, the cells were blocked with 2% FBS in PBS for 30 min at room temperature and incubated with the appropriate primary antibodies overnight at 4°C. After washing with PBS three times, the cells were incubated with Alexa-488- or Alexa-568-conjugated secondary antibodies in PBS containing 2% FBS or Can Get Signal immunostain solution A (Toyobo) for 1.5 h. Nuclear DNA was stained with DAPI. Fluorescence images were obtained using a fluorescence microscopy (DMi8, Leica

Microsystems), equipped with a PL Apo 63x oil immersion objective lens (NA 1.3) and a CMOS camera (C13440-20CU; Hamamatsu Photonics) driven by LAS AF Imaging Software (Leica Microsystems). Images were analyzed by using ImageJ.

In vitro kinase assay

Cells were washed with PBS and lysed with lysis buffer (50 mM Tris-HCl (pH7.5), 1% (v/v) Triton X-100, 150 mM NaCl, 5% (v/v) glycerol, 1 mM sodium vanadate, 1 mM DTT, 10 μg/ml leupeptin, and 3 μg/ml pepstatin A). Lysates were clarified by centrifugation at 15,000 rpm for 10 min at 4°C. The cell lysates were then pre-cleared with nProtein A Sepharose Fast Flow (GE Healthcare), and the supernatants were incubated with antibodies against NDR1/2 or LATS1/2 for 4 h at 4°C. After centrifugation, the beads were washed three times with wash buffer (500 mM NaCl, 50 mM Tris-HCl, 1% Triton X-100, 5% glycerol, and 1 mM DTT) and then washed twice with kinase buffer (20 mM Tris-HCl (pH 7.5), 10 mM $MgCl_2$, and 1 mM DTT). Kinase reactions were conducted in 20 μl of kinase buffer containing 50 μM ATP, 5 μCi [g-32P] ATP, and 1 μg of GST- YAP for 1 h at 30°C. GST-YAP was expressed in BL21 *Escherichia coli* and purified using glutathione-Sepharose. The reaction mixture was separated by SDS-PAGE and analyzed by autoradiography to quantitate the ^{32}P-labeled protein and by immunoblotting with anti-YAP and anti-NDR1/2 or LATS1/2 antibodies to detect the targeted proteins.

Subcellular fractionation

The nuclear/cytoplasmic fractionation was performed essentially according to (40). All the buffers used were kept on ice and centrifugations were done at 4°C with soft braking. HEK293A cells were grown on 10 cm culture dish at low density (1.6 x 10^4/cm^2) or high density (8.0 x 10^4/cm^2) for 24 h. After a single wash with PBS, cells were scraped with PBS and harvested by centrifugation at 1000 x g for 15 min. The cell pellet was gently resuspended with five times the volume of pellet with buffer-A (10 mM HEPES, pH 7.4, 1.5 mM $MgCl_2$, 10 mM KCl, and 0.5 mM DTT) and incubated on ice for 15 min, followed by homogenization (Wheaton) for 10 strokes. The cell lysates were centrifuged at 1000 x g for 5 min to collect the pellet as the nuclear fraction and the supernatant as the cytoplasmic fraction. The nuclear fraction was washed by centrifugation two times with buffer-A (1000 x g for 5 min each), resuspended with buffer-A to a similar volume as the cytoplasmic fraction and sonicated. Both fractions were boiled with sample buffer keeping an identical final volume and subjected to SDS-PAGE. Each fraction was immunoblotted for anti-YAP and anti-histone H3 antibodies.

Luciferase assay

For luciferase assay, cells were plated on 6-well plates and transfected with a combination of 500 ng of YAP/TAZ-responsive reporter 8xGTIIC-luciferase (34615, Addgene, Cambridge, MA) and 0.5 ng of control pcDNA-hRluc (referred to as Renilla luciferase) using jet PEI and cultured for 36 h. Cell lysates were generated and luciferase reactions were performed following the manufacturer's instruction, described in the Dual Luciferase Reporter Assay System (Promega, Madison, WI).

Statistical analysis

Statistical analysis included one-way analysis of variance (ANOVA) followed by Dunnett's test or Tukey's test for comparison of multiple data sets and was performed using Prism software version 6.0 c (GraphPad Software). Data represent the means of the indicated number of independent experiments. Error bars indicate the. standard deviation (SD)

Statistical significance was set at $p < 0.05$.

References

1. Zeng, Q., and Hong, W. (2008) The emerging role of the Hippo pathway in cell contact inhibition, organ size control, and cancer development in mammals. *Cancer Cell*. **13**, 188–192
2. Pan, D. (2010) The Hippo Signaling Pathway in Development and Cancer. *Dev. Cell*. **19**, 491–505
3. Yu, F.-X., Zhao, B., and Guan, K.-L. (2015) Hippo pathway in organ size control, tissue homeostasis, and cancer. *Cell*. **163**, 811–828
4. Harvey, K. F., Zhang, X., and Thomas, D. M. (2013) The Hippo pathway and human cancer. *Nat. Rev. Cancer*. **13**, 246–257
5. Moya, I. M., and Halder, G. (2019) Hippo–YAP/TAZ signalling in organ regeneration and regenerative medicine. *Nat. Rev. Mol. Cell Biol.* **20**, 211–226
6. Yu, F. X., and Guan, K. L. (2013) The Hippo pathway: Regulators and regulations. *Genes Dev.* **27**, 355–371
7. Schlegelmilch, K., Mohseni, M., Kirak, O., Pruszak, J., Rodriguez, J. R., Zhou, D., Kreger, B. T., Vasioukhin, V., Avruch, J., Brummelkamp, T. R., and Camargo, F. D. (2011) Yap1 acts downstream of α-catenin to control epidermal proliferation. *Cell*. **144**, 782–795
8. Zhao, B., Li, L., Wang, L., Wang, C. Y., Yu, J., and Guan, K. L. (2012) Cell detachment activates the Hippo pathway via cytoskeleton reorganization to induce anoikis. *Genes Dev.* **26**, 54–68
9. Wada, K.-I., Itoga, K., Okano, T., Yonemura, S., and Sasaki, H. (2011) Hippo pathway regulation by cell morphology and stress fibers. *Development*. **138**, 3907–3914
10. Sansores-Garcia, L., Bossuyt, W., Wada, K.-I., Yonemura, S., Tao, C., Sasaki, H., and Halder, G. (2011) Modulating F-actin organization induces organ growth by affecting the Hippo pathway. *EMBO J.* **30**, 2325–2335
11. Aragona, M., Panciera, T., Manfrin, A., Giulitti, S., Michielin, F., Elvassore, N., Dupont, S., and Piccolo, S. (2013) A mechanical checkpoint controls multicellular growth through YAP/TAZ regulation by actin-processing factors. *Cell*. **154**, 1047–1059
12. Zhou, D., Conrad, C., Xia, F., Park, J. S., Payer, B., Yin, Y., Lauwers, G. Y., Thasler, W., Lee, J. T., Avruch, J., and Bardeesy, N. (2009) Mst1 and Mst2 maintain hepatocyte quiescence and suppress hepatocellular carcinoma development through inactivation of the Yap1 oncogene. *Cancer Cell*. **16,** 425–438.
13. Dupont, S., Morsut, L., Aragona, M., Enzo, E., Giulitti, S., Cordenonsi, M., Zanconato, F., Le Digabel, J., Forcato, M., Bicciato, S., Elvassore, N., and Piccolo, S. (2011) Role of YAP/TAZ in mechanotransduction. *Nature*. **474**, 179–183
14. Kim, J., Jo, H., Hong, H., Kim, M. H., Kim, J. M., Lee, J.-K., Heo, W. Do, and Kim, J. (2015) Actin remodelling factors control ciliogenesis by regulating YAP/TAZ activity and vesicle trafficking. *Nat. Commun.* **6**, 6781
15. Nagai, T., and Mizuno, K. (2017) Jasplakinolide induces primary cilium formation through cell rounding and YAP inactivation. *PLoS One*. **12**, e0183030
16. Hergovich, A., Stegert, M. R., Schmitz, D., and Hemmings, B. A. (2006) NDR kinases regulate essential cell processes from yeast to humans. *Nat. Rev. Mol. Cell Biol.* **7**, 253–264
17. Sharif, A. A. D., and Hergovich, A. (2018) The NDR/LATS protein kinases in immunology and cancer biology. *Semin. Cancer Biol.* **48**, 104–114

18. Zhang, L., Tang, F., Hergovich, A., Schmitz-rohmer, D., Zhang, L., Tang, F., Terracciano, L., Hynx, D., Kohler, R., Bichet, S., and Hess, D. (2015) NDR functions as a physiological YAP1 kinase in the intestinal epithelium. *Curr. Biol.* **25**, 296–305
19. Du, L., and Novick, P. (2002) Pag1p , a novel protein associated with protein kinase Cbk1p , is required for cell morphogenesis and proliferation in Saccharomyces cerevisiae. *Mol. Biol. Cell.* **13**, 503–514
20. He, Y., Fang, X., Emoto, K., Jan, Y.-N., and Adler, P. N. (2004) The Tricornered Ser/Thr protein kinase is regulated by phosphorylation and interacts with Furry during *Drosophila* wing hair development. *Mol. Biol. Cell*. **16**, 689–700
21. Chiba, S., Ikeda, M., Katsunuma, K., Ohashi, K., and Mizuno, K. (2009) MST2- and Furry-mediated activation of NDR1 kinase is critical for precise alignment of mitotic chromosomes. *Curr. Biol.* **19**, 675–681
22. Nagai, T., and Mizuno, K. (2014) Multifaceted roles of furry proteins in invertebrates and vertebrates. *J. Biochem.* **155**, 137–146
23. Hirata, D., Kishimoto, N., Suda, M., Sogabe, Y., Nakagawa, S., Yoshida, Y., Sakai, K., Mizunuma, M., Miyakawa, T., Ishiguro, J., and Toda, T. (2002) Fission yeast Mor2/Cps12, a protein similar to Drosophila Furry, is essential for cell morphogenesis and its mutation induces Wee1-dependent G(2) delay. *EMBO J.* **21**, 4863–4874
24. Gallegos, M. E., and Bargmann, C. I. (2004) Mechanosensory neurite termination and tiling depend on SAX-2 and the SAX-1 kinase. *Neuron*. **14**, 239–249
25. Cong, J., Geng, W., He, B., Liu, J., Charlton, J., and Adler, P. N. (2001) The furry gene of Drosophila is important for maintaining the integrity of cellular extensions during morphogenesis. *Development*. **2802**, 2793–2802
26. Emoto, K., He, Y., Ye, B., Grueber, W. B., Adler, P. N., Jan, L. Y., and Jan, Y.-N. (2004) Control of dendritic branching and tiling by the Tricornered-kinase/Furry signaling pathway in Drosophila sensory neurons. *Cell*. **119**, 245–256
27. Zhao, B., Zhao, B., Wei, X., Wei, X., Li, W., Li, W., Udan, R. S., Udan, R. S., Yang, Q., Yang, Q., Kim, J., Kim, J., Xie, J., Xie, J., Ikenoue, T., Ikenoue, T., Yu, J., Yu, J., Li, L., Li, L., Zheng, P., Zheng, P., Ye, K., Ye, K., Chinnaiyan, A., Chinnaiyan, A., Halder, G., Halder, G., Lai, Z., Lai, Z., Guan, K.-L., and Guan, K.-L. (2007) Inactivation of YAP oncoprotein by the Hippo pathway is involved in cell contact inhibition and tissue growth control. *Genes Dev.* **21**, 2747–2761
28. Zhao, B., Kim, J., Ye, X., Lai, Z. C., and Guan, K. L. (2009) Both TEAD-binding and WW domains are required for the growth stimulation and oncogenic transformation activity of yes-associated protein. *Cancer Res.* **69**, 1089–1098
29. Xiong, S., Lorenzen, K., Couzens, A. L., Templeton, C. M., Rajendran, D., Mao, D. Y. L., Juang, Y. C., Chiovitti, D., Kurinov, I., Guettler, S., Gingras, A. C., and Sicheri, F. (2018) Structural basis for auto-inhibition of the NDR1 kinase domain by an atypically long activation segment. *Structure*.
30. Hergovich, A., Lamla, S., Nigg, E. a, and Hemmings, B. a (2007) Centrosome-associated NDR kinase regulates centrosome duplication. *Mol. Cell*. **25**, 625–634
31. Cornils, H., Stegert, M. R., Hergovich, A., Hynx, D., Schmitz, D., Dirnhofer, S., and Hemmings, B. A. (2010) Ablation of the kinase NDR1 predisposes mice to the development of T cell lymphoma. *Sci. Signal.* **3**, 1–15
32. Cornils, H., Kohler, R. S., Hergovich, A., and Hemmings, B. A. (2011) Human NDR kinases control G1/S cell

cycle transition by directly regulating p21 stability. *Mol. Cell. Biol.* **31**, 1382–1395

33. Ren, X., Graham, J. C., Jing, L., Mikheev, A. M., Gao, Y., Lew, J. P., Xie, H., Kim, A. S., Shang, X., Friedman, C., Vail, G., Fang, M. Z., Bromberg, Y., and Zarbl, H. (2013) Mapping of Mcs30, a new mammary carcinoma susceptibility quantitative trait locus (QTL30) on rat chromosome 12: identification of Fry as a candidate Mcs gene. *PLoS One*. **8**, 1–12
34. Liu, Y., Chen, X., Gong, Z., Zhang, H., Fei, F., Tang, X., Wang, J., Xu, P., Zarbl, H., and Ren, X. (2019) Fry is required for mammary gland development during pregnant periods and affects the morphology and growth of breast cancer cells. *Front. Oncol.* **9**, 1–12
35. Najmabadi, H., Hu, H., Garshasbi, M., Zemojtel, T., Abedini, S. S., Chen, W., Hosseini, M., Behjati, F., Haas, S., Jamali, P., Zecha, A., Mohseni, M., Püttmann, L., Vahid, L. N., Jensen, C., Moheb, L. A., Bienek, M., Larti, F., Mueller, I., Weissmann, R., Darvish, H., Wrogemann, K., Hadavi, V., Lipkowitz, B., Esmaeeli-Nieh, S., Wieczorek, D., Kariminejad, R., Firouzabadi, S. G., Cohen, M., Fattahi, Z., Rost, I., Mojahedi, F., Hertzberg, C., Dehghan, A., Rajab, A., Banavandi, M. J. S., Hoffer, J., Falah, M., Musante, L., Kalscheuer, V., Ullmann, R., Kuss, A. W., Tzschach, A., Kahrizi, K., and Ropers, H. H. (2011) Deep sequencing reveals 50 novel genes for recessive cognitive disorders. *Nature*. **478**, 57–63
36. Chiba, S., Amagai, Y., Homma, Y., Fukuda, M., and Mizuno, K. (2013) NDR2-mediated Rabin8 phosphorylation is crucial for ciliogenesis by switching binding specificity from phosphatidylserine to Sec15. *EMBO J.* **32**, 874–85
37. Ikeda, M., Chiba, S., Ohashi, K., and Mizuno, K. (2012) Furry protein promotes aurora A-mediated Polo-like kinase 1 activation. *J. Biol. Chem.* **287**, 27670–81
38. Shalem, O., Sanjana, E. N., Hartenian, E., and Zhang, F. (2014) Genome-Scale CRISPR-Cas9 Knockout. *Science.* **343**, 84–87
39. Ran, F., Hsu, P., Wright, J., and Agarwala, V. (2013) Genome engineering using the CRISPR-Cas9 system. *Nat. Protoc.* **8**, 2281–308
40. Das, A., Fischer, R. S., Pan, D., and Waterman, C. M. (2016) YAP nuclear localization in the absence of cell-cell contact is mediated by a filamentous actin-dependent , Myosin II- and phospho-YAP-independent pathway during extracellular matrix mechanosensing. *J. Biol. Chem.* **291**, 6096–6110

Figure legends

Figure 1. FRY depletion promotes YAP nuclear localization.

(A) Validation of FRY knockout (KO) in HEK293A cells. Lysates of parental cells (PC) and two independently derived FRY-KO cell lines (#1 and #2) were immunoprecipitated and immunoblotted using an anti-FRY antibody. Cell lysates were analyzed by immunoblotting with an anti-α-tubulin antibody.

(B) Effects of FRY depletion on the nuclear/cytoplasmic localization of YAP. Cells were cultured at low density (1.6 x 10^4/cm^2) or high density (8.0 x 10^4/cm^2) for 24 hours. The parental and FRY-KO cells were cultured at low and high cell densities under serum-supplemented conditions and stained using an anti-YAP antibody (green) and DAPI (blue). Scale bar, 20 μm.

(C) Quantification of the effects of FRY depletion on YAP nuclear localization. The number of cells with YAP localization in the nucleus (preferentially in the nucleus or equally in the nucleus and cytoplasm) were counted and the percentages calculated. Data are the means ± SD. from three independent experiments with more than 100 cells evaluated for each experiment. Statistical analysis included one-way ANOVA followed by Dunnett's test. **$p < 0.01$; N.S., not significant.

(D) FRY KO 293A cells were transfected with an 8xGTIIC-luciferase YAP-dependent promoter plasmid and a plasmid with the SV40 promoter driving Renilla luciferase for 36 hours. Cell extracts were made, and luciferase activity was measured for each sample. The levels of firefly luciferase (YAP activity) were normalized to the level of Renilla luciferase in each sample. Error bars indicate the SD among four independent experiments. Brackets on top of bars represent statistical significance (Dunnet's test, *$p < 0.05$, **$p < 0.01$).

(E) Effects of FRY depletion on the nuclear/cytoplasmic localization of TAZ. The parental and FRY-KO cells were cultured at low and high cell densities under serum-supplemented conditions and stained using an anti-TAZ antibody (green) and DAPI (blue). Scale bar, 20 μm.

(F) Quantification of the effects of FRY depletion on TAZ nuclear localization. The number of cells with TAZ localization in the nucleus (preferentially in the nucleus or equally in the nucleus and cytoplasm) were counted and the percentages calculated. Data are the means ± SD. from three independent experiments with more than 100 cells evaluated for each experiment. Statistical analysis included one-way ANOVA followed by Dunnett's test. **$p < 0.01$; N.S., not significant.

Figure 2. FRY depletion decreases NDR1/2 kinase activities and YAP phosphorylation.

(A) Effects of FRY depletion on kinase activities of NDR1 and NDR2. Parental or FRY-KO HEK293A cells were cultured at high density under serum-supplemented conditions. NDR1 and NDR2 were immunoprecipitated from cell lysates and subjected to in vitro kinase assays using GST-YAP as a substrate. IgG HC, immunoglobulin heavy chain.

(B) Effects of FRY depletion on kinase activities of LATS1 and LATS2. LATS1 and LATS2 were immunoprecipitated and subjected to in vitro kinase assays as in (A).

(C) Effects of FRY depletion on the level of YAP phosphorylation. The parental or FRY-KO HEK293A cells were cultured at high density under serum-supplemented conditions. Cell lysates were analyzed by immunoblotting using anti-pS127-YAP (phospho-Ser-127), anti-YAP, and anti-α-tubulin antibodies.

(D) Quantification of the ratio of pS127-YAP to total YAP. The relative ratios of pS127-YAP/YAP were determined by densitometric analysis of the immunoblot data. Data are the means ± SD from three independent experiments. Statistical analysis included one-way ANOVA followed by Dunnett's test. **$p < 0.01$.

Figure 3. Knockdown of NDR1/2 decreases YAP phosphorylation and promotes YAP nuclear localization.

(A) Effects of NDR1/2-targeting siRNAs on the expression of NDR1 and NDR2. HEK293A cells were transfected with control siRNA (siCtrl), a mixture of NDR1 siRNA #1 and NDR2 siRNA #1 (siNDR1/2 #1), or a mixture of NDR1 siRNA #2 and NDR2 siRNA #2 (siNDR1/2 #2) and then cultured for 48 h. For detection of NDR1, cell lysates were analyzed by immunoblotting using an anti-NDR1 antibody. For detection of NDR2, cell lysates were immunoprecipitated and immunoblotted using an anti-NDR2 antibody. Cell lysates were also analyzed by immunoblotting using an anti-a-tubulin antibody. IgG HC, immunoglobulin heavy chain.

(B) Effects of NDR1/2 knockdown on YAP phosphorylation. HEK293A cells were transfected with control siRNA (siCtrl) or a mixture of NDR1 and NDR2 siRNAs (siNDR1/2) and the cell lysates were subjected to immunoblotting using anti-pS127-YAP, anti-YAP, and anti-α-tubulin antibodies.

(C) Quantification of the ratio of pS127-YAP to YAP. Data are the means ± SD from three independent experiments. Statistical analysis included one-way ANOVA followed by Dunnett's test. *$p < 0.05$, **$p < 0.01$.

(D) Effects of LATS1/2-targeting siRNAs on the expression of LATS1 and LATS2. HEK293A cells were transfected with control siRNA (siCtrl), a mixture of LATS1 siRNA #1 and LATS2 siRNA #1 (siLATS1/2 #1), or a mixture of LATS1 siRNA #2 and LATS2 siRNA #2 (siLATS1/2 #2) and then cultured for 48 h.

(E) Effects of NDR1/2 knockdown on the nuclear/cytoplasmic localization of YAP in parental and FRY-KO HEK293A cells. The parental and FRY- KO cells were transfected with control siRNA (siCtrl) or a mixture of NDR1 and NDR2 siRNAs (siNDR1/2) and then cultured for 48 h at a high cell density under serum-supplemented conditions. The cells were stained with an anti-YAP antibody (green) and DAPI (blue). Scale bar, 20 μm.

(F) Quantification of the effects of NDR1/2 knockdown on YAP localization. The percentage of cells with YAP localization in the nucleus was determined as described in Fig. 1C. Data are the means ± SD from three independent experiments with more than 100 cells evaluated for each experiment. Statistical analysis included one-way ANOVA followed by Tukey's test. *$p < 0.05$, **$p < 0.01$, N.S., not significant.

(G) Effects of LATS1/2 knockdown on the nuclear/cytoplasmic localization of YAP in parental and FRY-KO HEK293A cells. Scale bar, 20 μm. C, quantification of the effects LATS1/2 knockdown on the nuclear/cytoplasmic localization of YAP in parental and FRY-KO HEK293A cells. The percentage of cells with nuclear localization of YAP was determined as described in Fig. 1C. Data are the means ± SD from three independent experiments with more than 100 cells evaluated for each experiment. Statistical analysis included one- way ANOVA followed by Tukey's test. *$p < 0.05$, **$p < 0.01$; N.S., not significant.

Figure 4. FRY binds to YAP through the N-terminal region.

(A) FRY binds to YAP. HEK293T cells were co-transfected with GFP-YAP and FRY-(Myc+His). Cell lysates were immunoprecipitated using an anti-GFP antibody and the precipitates were immunoblotted using anti-GFP and anti-Myc antibodies.

(B) Interaction between endogenous FRY and YAP. Lysates of HEK293A cells were immunoprecipitated using an anti-FRY antibody and the precipitates were analyzed by immunoblotting using anti-YAP and anti-FRY antibodies.

(C) Schematic structures of FRY and its fragments. The numbers indicate the amino acid residues for the N-terminal (N), middle region (M), and C-terminal (C) fragments.

(D) The interaction between YAP and FRY fragments. HEK293T cells were co-transfected with GFP-YAP and (Myc+His)-tagged FRY fragments. Cell lysates were immunoprecipitated using an anti-GFP antibody and the precipitates

were analyzed by immunoblotting using anti-GFP and anti-Myc antibodies.
(E) FRY interacts with YAP through the middle region.
(F) FRY binds to a non- phosphorylated 5SA mutant of YAP. HEK293T cells were transfected with GFP-YAP (WT or 5SA) and FRY-(Myc+His). Cell lysates were immunoprecipitated using an anti-GFP antibody and the precipitates were immunoblotted using anti-GFP and anti-Myc antibodies.

Figure 5. Expression of FRY or its N-terminal fragment recovers YAP cytoplasmic localization in FRY-KO cells.
(A) Effects of expression of FRY or its fragments on YAP nuclear localization in FRY-KO cells. Parental or FRY-KO HEK293A cells were transfected with control GFP, (Myc+His)-tagged full- length (FL) FRY, or its fragments and then fixed and stained using an anti-YAP antibody (red). In the first and second rows, cells were imaged for GFP fluorescence (green). In the third to fifth rows, cells were stained with an anti-Myc antibody (green). DNA was stained using DAPI (blue). Arrows indicate the GFP- or Myc-positive cells. Scale bar, 20 μm.
(B) Quantification of the effects of expression of FRY or its fragments on YAP nuclear localization. The percentage of cells with nuclear localization of YAP was determined as described in Fig. 1C. Data are the means ± SD from three independent experiments with more than 30 cells evaluated for each experiment. Statistical analysis included one- way ANOVA followed by Tukey's test. *$p < 0.05$, **$p < 0.01$; N.S., not significant.
(C) Effects of expression of FRY fragments on YAP nuclear localization in FRY-KO cells. Scale bar, 20 μm.
(D) Quantification of the effects of expression of FRY or its fragments on YAP nuclear localization. The percentage of cells with nuclear localization of YAP was determined as described in Fig. 1C. Data are the means ± SD. from three independent experiments with more than 30 cells evaluated for each experiment. Statistical analysis included one- way ANOVA followed by Tukey's test. *$p < 0.05$, **$p < 0.01$; N.S., not significant.

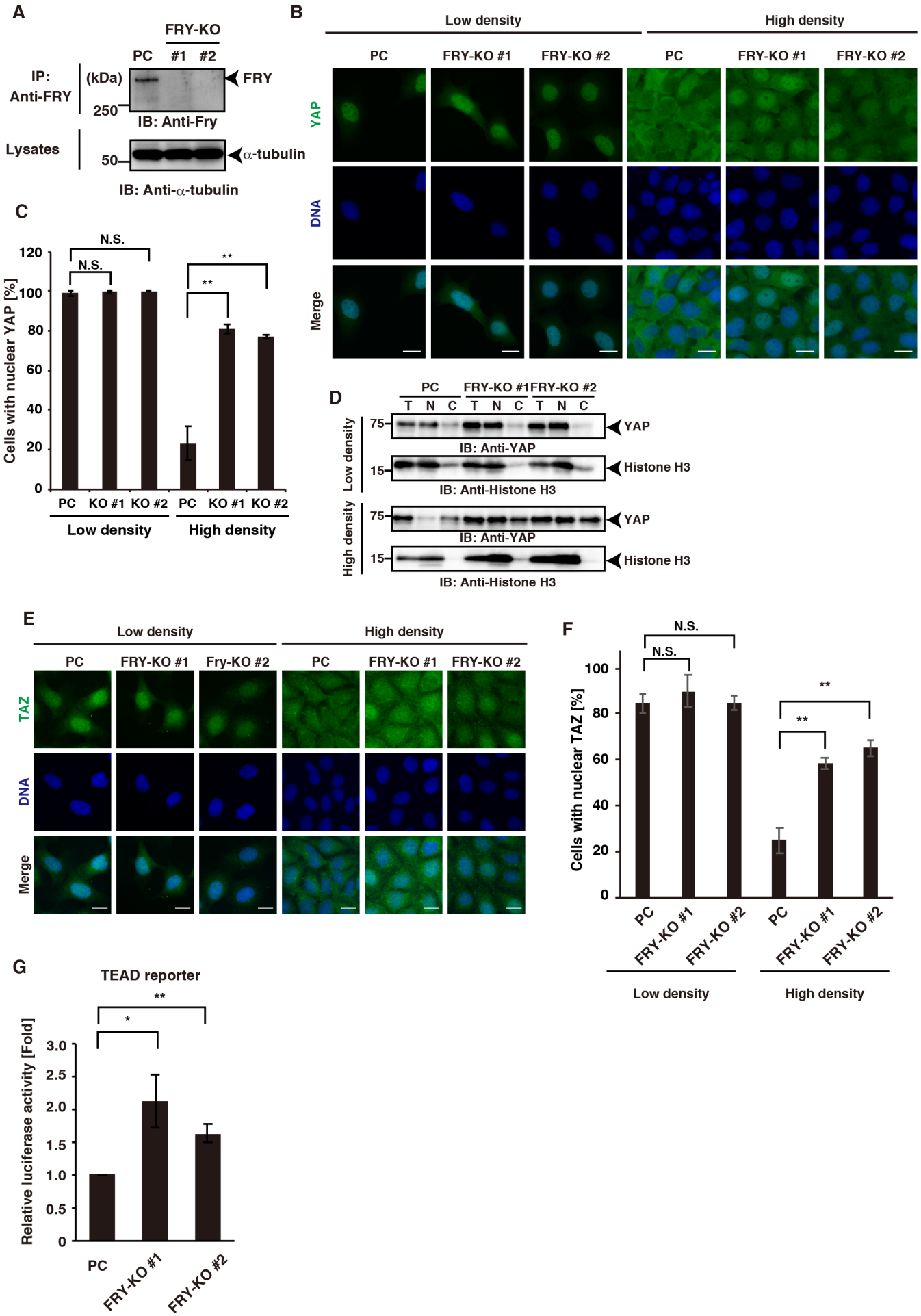
A
FRY-KO
PC
#1
#2
IP:
Anti-FRY
(kDa)
250
FRY
IB: Anti-Fry
Lysates
50
α-tubulin
IB: Anti-α-tubulin
B
Low density
High density
PC
FRY-KO #1
FRY-KO #2
YAP
DNA
Merge
C
Cells with nuclear YAP [%]
N.S.
**
PC
KO #1
KO #2
Low density
High density
D
PC
FRY-KO #1
FRY-KO #2
T
N
C
Low density
High density
75
15
YAP
Histone H3
IB: Anti-YAP
IB: Anti-Histone H3
E
TAZ
DNA
Merge
Fry-KO #2
F
Cells with nuclear TAZ [%]
G
TEAD reporter
Relative luciferase activity [Fold]
*

Fig.1

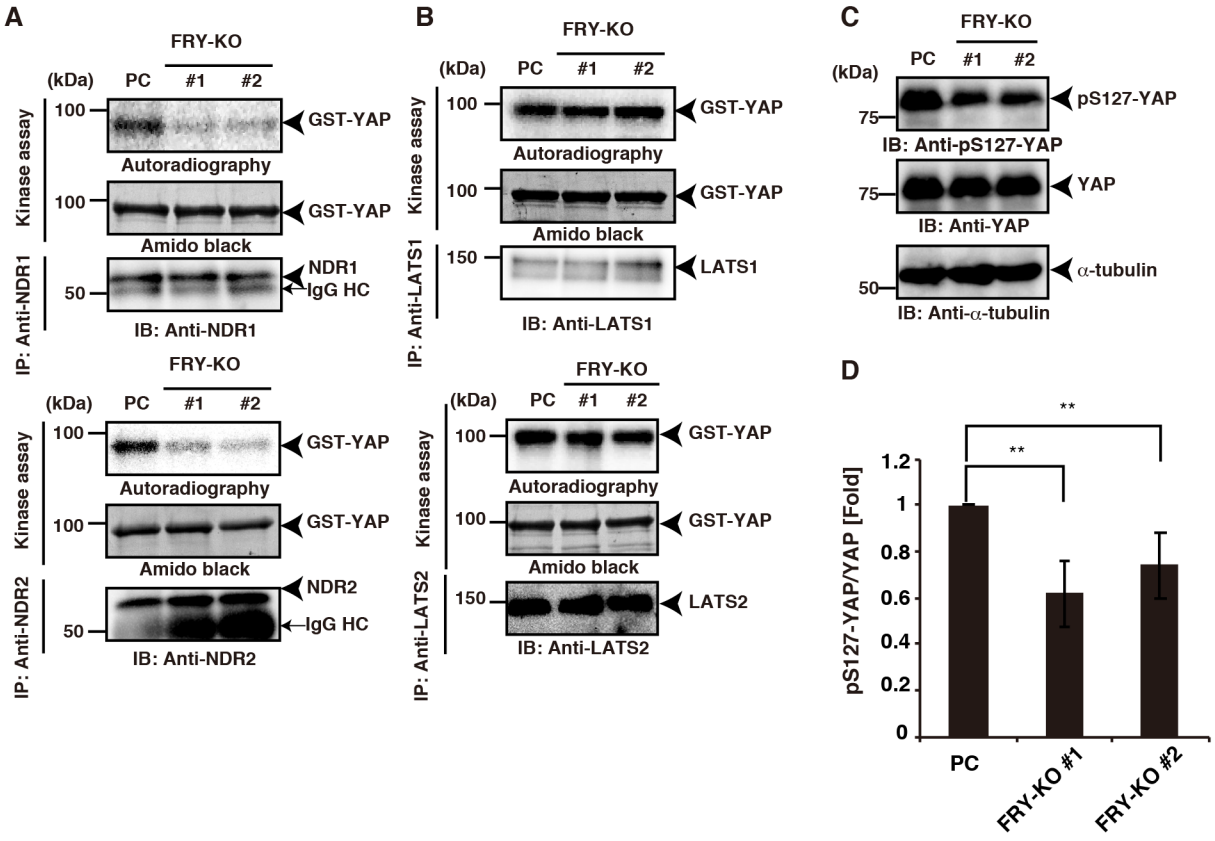
A
FRY-KO
(kDa)
PC
#1
#2
Kinase assay
100
GST-YAP
Autoradiography
100
GST-YAP
Amido black
IP: Anti-NDR1
50
NDR1
IgG HC
IB: Anti-NDR1
FRY-KO
(kDa)
PC
#1
#2
Kinase assay
100
GST-YAP
Autoradiography
100
GST-YAP
Amido black
IP: Anti-NDR2
50
NDR2
IgG HC
IB: Anti-NDR2
B
FRY-KO
(kDa)
PC
#1
#2
Kinase assay
100
GST-YAP
Autoradiography
100
GST-YAP
Amido black
IP: Anti-LATS1
150
LATS1
IB: Anti-LATS1
FRY-KO
(kDa)
PC
#1
#2
Kinase assay
100
GST-YAP
Autoradiography
100
GST-YAP
Amido black
IP: Anti-LATS2
150
LATS2
IB: Anti-LATS2
C
FRY-KO
(kDa)
PC
#1
#2
75
pS127-YAP
IB: Anti-pS127-YAP
75
YAP
IB: Anti-YAP
50
α-tubulin
IB: Anti-α-tubulin
D
**
**
pS127-YAP/YAP [Fold]
1.2
1
0.8
0.6
0.4
0.2
0
PC
FRY-KO #1
FRY-KO #2

Fig.2

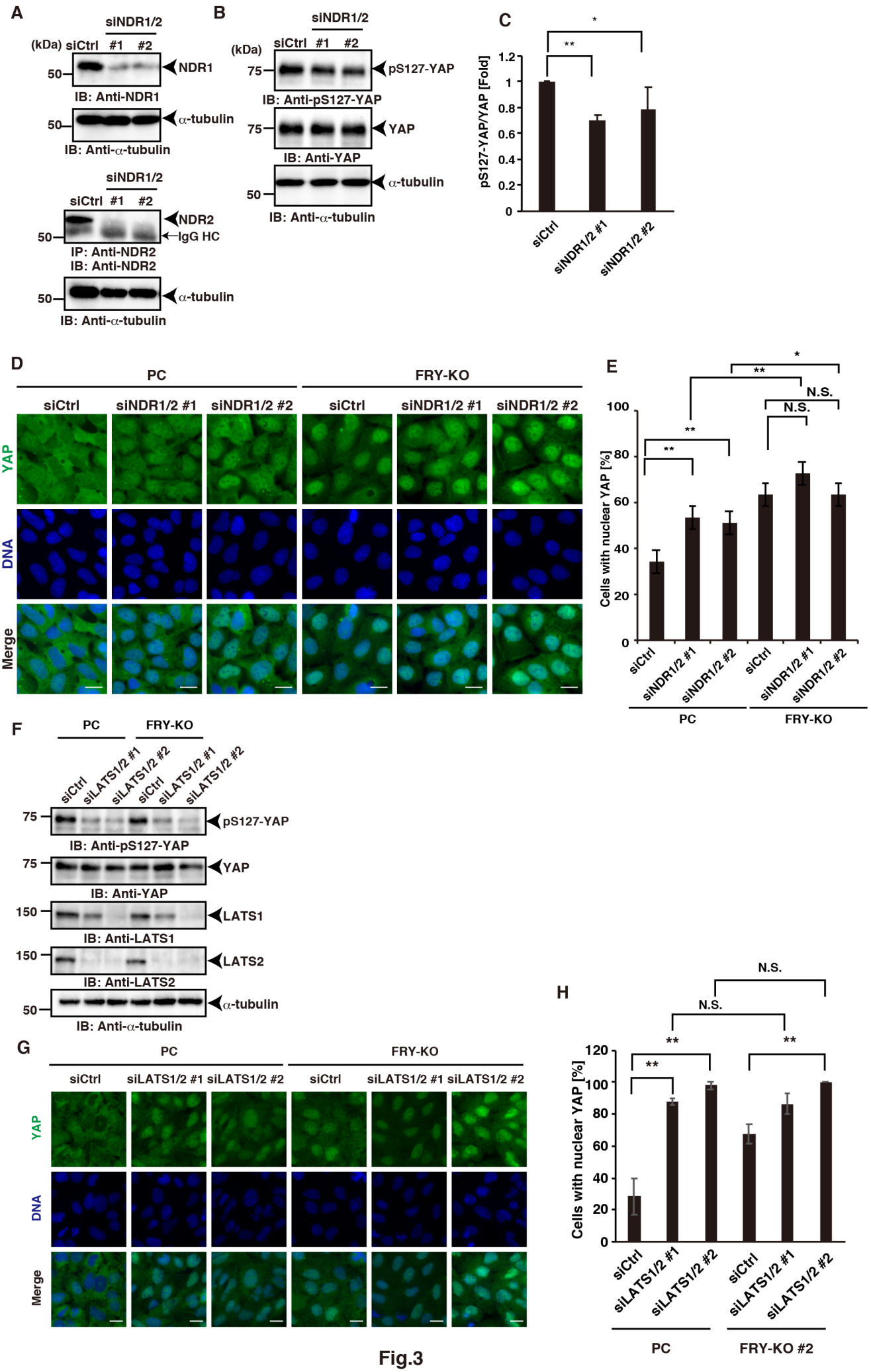
A
siNDR1/2
(kDa) siCtrl #1 #2
50
NDR1
IB: Anti-NDR1
50
α-tubulin
IB: Anti-α-tubulin
siNDR1/2
siCtrl #1 #2
50
NDR2
IgG HC
IP: Anti-NDR2
IB: Anti-NDR2
50
α-tubulin
IB: Anti-α-tubulin
B
siNDR1/2
(kDa)
siCtrl #1 #2
75
pS127-YAP
IB: Anti-pS127-YAP
75
YAP
IB: Anti-YAP
50
α-tubulin
IB: Anti-α-tubulin
C
*
**
pS127-YAP/YAP [Fold]
1.2
1
0.8
0.6
0.4
0.2
0
siCtrl
siNDR1/2 #1
siNDR1/2 #2
D
PC
FRY-KO
siCtrl
siNDR1/2 #1
siNDR1/2 #2
siCtrl
siNDR1/2 #1
siNDR1/2 #2
YAP
DNA
Merge
E
*
**
N.S.
N.S.
**
**
Cells with nuclear YAP [%]
100
80
60
40
20
0
siCtrl
siNDR1/2 #1
siNDR1/2 #2
siCtrl
siNDR1/2 #1
siNDR1/2 #2
PC
FRY-KO
F
PC
FRY-KO
siCtrl
siLATS1/2 #1
siLATS1/2 #2
siCtrl
siLATS1/2 #1
siLATS1/2 #2
75
pS127-YAP
IB: Anti-pS127-YAP
75
YAP
IB: Anti-YAP
150
LATS1
IB: Anti-LATS1
150
LATS2
IB: Anti-LATS2
50
α-tubulin
IB: Anti-α-tubulin
G
PC
FRY-KO
siCtrl
siLATS1/2 #1 siLATS1/2 #2
siCtrl
siLATS1/2 #1 siLATS1/2 #2
YAP
DNA
Merge
H
N.S.
N.S.
**
**
**
Cells with nuclear YAP [%]
120
100
80
60
40
20
0
siCtrl
siLATS1/2 #1
siLATS1/2 #2
siCtrl
siLATS1/2 #1
siLATS1/2 #2
PC
FRY-KO #2

Fig.3

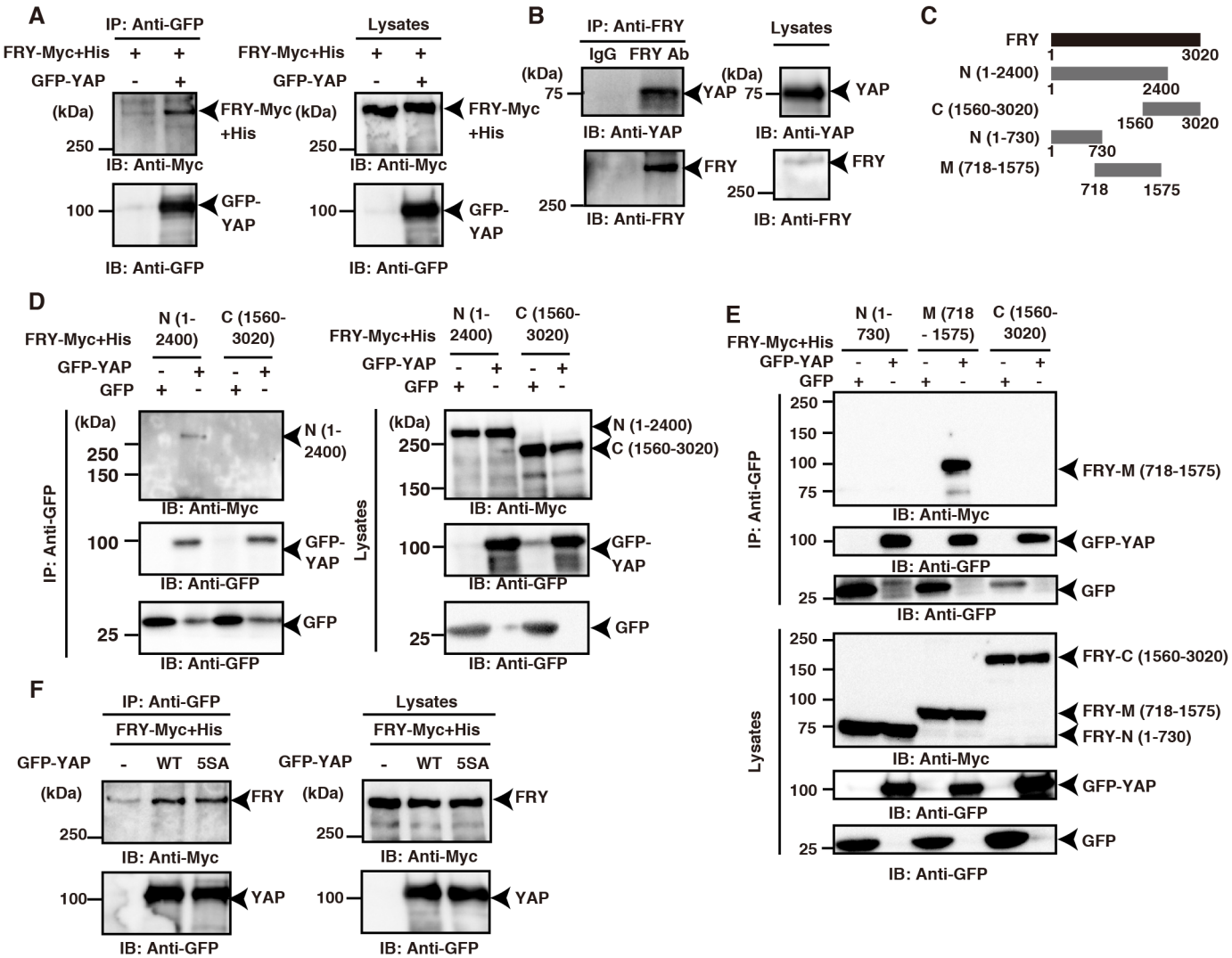
A
IP: Anti-GFP
FRY-Myc+His + +
GFP-YAP - +
(kDa)
250
FRY-Myc +His
IB: Anti-Myc
100
GFP-YAP
IB: Anti-GFP
Lysates
FRY-Myc+His + +
GFP-YAP - +
(kDa)
250
FRY-Myc +His
IB: Anti-Myc
100
GFP-YAP
IB: Anti-GFP
B
IP: Anti-FRY
IgG FRY Ab
(kDa)
75
YAP
IB: Anti-YAP
FRY
250
IB: Anti-FRY
Lysates
(kDa)
75
YAP
IB: Anti-YAP
FRY
250
IB: Anti-FRY
C
FRY
1
3020
N (1-2400)
1
2400
C (1560-3020)
1560
3020
N (1-730)
1
730
M (718-1575)
718
1575
D
FRY-Myc+His
N (1-2400)
C (1560-3020)
GFP-YAP - + - +
GFP + - + -
IP: Anti-GFP
(kDa)
250
150
N (1-2400)
IB: Anti-Myc
100
GFP-YAP
IB: Anti-GFP
25
GFP
IB: Anti-GFP
Lysates
(kDa)
250
150
N (1-2400)
C (1560-3020)
IB: Anti-Myc
100
GFP-YAP
IB: Anti-GFP
25
GFP
IB: Anti-GFP
E
FRY-Myc+His
N (1-730)
M (718-1575)
C (1560-3020)
GFP-YAP - + - + - +
GFP + - + - + -
IP: Anti-GFP
250
150
100
75
FRY-M (718-1575)
IB: Anti-Myc
100
GFP-YAP
IB: Anti-GFP
25
GFP
IB: Anti-GFP
Lysates
250
150
100
75
FRY-C (1560-3020)
FRY-M (718-1575)
FRY-N (1-730)
IB: Anti-Myc
100
GFP-YAP
IB: Anti-GFP
25
GFP
IB: Anti-GFP
F
IP: Anti-GFP
FRY-Myc+His
GFP-YAP - WT 5SA
(kDa)
250
FRY
IB: Anti-Myc
100
YAP
IB: Anti-GFP
Lysates
FRY-Myc+His
GFP-YAP - WT 5SA
(kDa)
250
FRY
IB: Anti-Myc
100
YAP
IB: Anti-GFP

Fig. 4

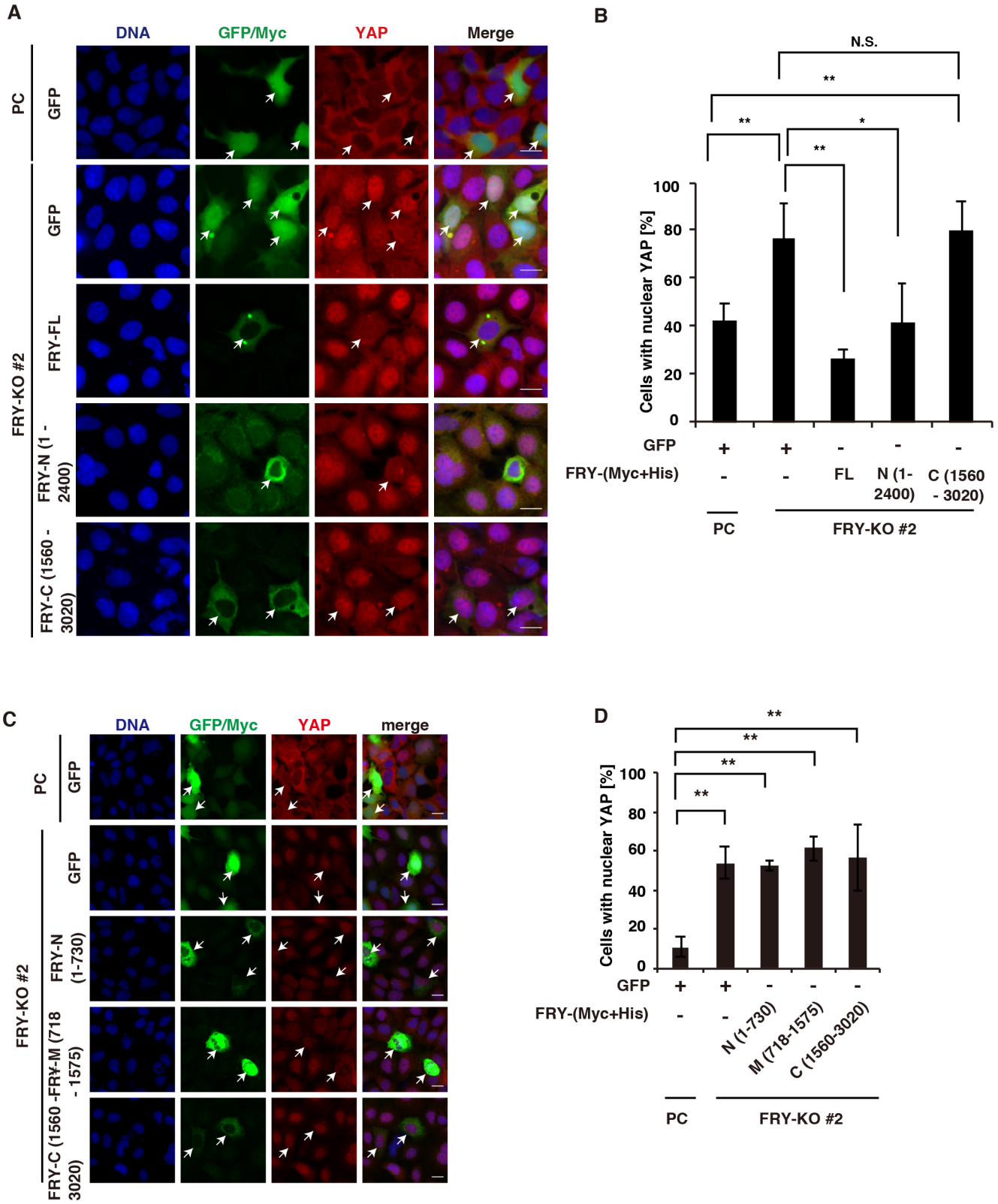
A
DNA
GFP/Myc
YAP
Merge
PC
GFP
FRY-KO #2
GFP
FRY-FL
FRY-N (1 - 2400)
FRY-C (1560 - 3020)
B
N.S.
**
**
*
**
Cells with nuclear YAP [%]
100
80
60
40
20
0
GFP
+
+
-
-
-
FRY-(Myc+His)
-
-
FL
N (1-2400)
C (1560 - 3020)
PC
FRY-KO #2
C
DNA
GFP/Myc
YAP
merge
PC
GFP
FRY-KO #2
GFP
FRY-N (1-730)
FRY-M (718 - 1575)
FRY-C (1560 - 3020)
D
**
**
**
**
Cells with nuclear YAP [%]
100
80
60
40
20
0
GFP
+
+
-
-
-
FRY-(Myc+His)
-
-
N (1-730)
M (718-1575)
C (1560-3020)
PC
FRY-KO #2

Fig. 5

Chapter II

Involvements of 14-3-3 proteins in CEP97 degradation

Abstract

Primary cilia are microtubule-based antenna-like structures that transmit various extracellular signals. Primary cilia play critical roles in the development and homeostasis of many tissues, and dysfunctions of primary cilia are associated with many human diseases. Centriolar protein CP110 and its interactor CEP97 localize to the distal end of the mother centriole and suppress inappropriate ciliogenesis by blocking axonemal microtubule assembly; therefore, removal of the CP110-CEP97 complex from the mother centriole is required for initiating axoneme extension and ciliogenesis. A previous study in our laboratory showed that CEP97 is degraded upon serum starvation by the ubiquitin-proteasome system and that the CUL3-RBX1-KCTD10 complex acts as the E3 ubiquitin ligase responsible for CEP97 ubiquitination and degradation, in which KCTD10 links CEP97 to CUL3-RBX1 complex. To understand the mechanism regulating the serum-starvation-induced CEP97 degradation, I searched for KCTD10-binding proteins and identified 14-3-3 proteins as the KCTD10 interactor. I also showed that 14-3-3-β binds to CEP97. Treatment with lambda protein phosphatase suppressed these interactions, indicating that 14-3-3-β binds to KCTD10 and CEP97 in a phosphorylation-dependent manner. I also showed that CEP97-KCTD10 interaction is increased by the inhibitor of protein phosphatases and blocked by a dominant-negative form of 14-3-3-β, suggesting that 14-3-3 proteins serve as a linker to stimulate the interaction between CEP97 and KCTD10, dependent on their phosphorylation. The level of the phosphorylated CEP97 was increased by the treatment with MG-132, an inhibitor of proteasome, in serum-starved cells, suggesting that CEP97 phosphorylation is involved in its degradation. I showed that the amount of CEP97 bound to 14-3-3-β was increased upon serum starvation and that the overexpression of a dominant-negative form of 14-3-3-β suppressed CEP97 ubiquitination, suggesting that CEP97 binding to 14-3-3 proteins is involved in the serum-starvation-induced CEP97 ubiquitination and degradation. Furthermore, overexpression of a dominant-negative form of 14-3-3-β suppressed CEP97 removal from the mother centriole and ciliogenesis. Taken together, these results suggest that 14-3-3 proteins play crucial roles in CEP97 removal from the mother centriole and consequent ciliogenesis by promoting the CEP97-KCTD10 interaction and CEP97 ubiquitination and degradation.

Introduction

Primary cilia are antenna-like protrusions that extend from the cell surface and are present in most vertebrate cell type. Numerous ion channels and receptors, such as those for hedgehog and PDGF signaling, are enriched in the membrane of primary cilia (1). Primary cilia sense fluid flow and extracellular signals and transduce these signals to regulate various physiological processes, including left-right patterning, calcium flux in kidney cells and and osteogenic differentiation in mesenchymal stem cells. Primary cilia are essential for development, such as formation of brain and limb. The defects in the formation and function of cilia result in serious developmental disorders, called ciliopathies, including nephronophthisis (NPHP), Joubert syndrome (JBTS), and Meckel syndrome (MKS) (2).

Primary cilia extend a microtubule-based axoneme from the basal body derived from the mother centriole. The mother centriole, but not the daughter centriole, contains the distal and sub-distal appendages. These centrioles duplicate once per cell cycle in most cell types. Two centrioles and the pericentriolar matrix form the centrosome, which functions as a microtubule-organizing center in interphase cells and a major organizer of spindle microtubules in mitotic cells. Primary cilia typically form at G1/G0 phase of cell cycle by ordered sequence of steps and disassemble during re-entry to cell cycle (3, 4). Upon serum starvation, ciliary vesicles derived from the Golgi apparatus and recycling endosomes accumulate to the vicinity of distal appendages of the mother centriole, and dock at the centriole to initiate transition from the mother centriole to the basal body (5). After fusion with the plasma membrane, the basal body nucleates axoneme microtubules, in a manner dependent on intraflagellar transport (IFT) (6). IFT transport is bi-directional, anterograde (from the base to the tip of the cilium via kinesin-2) and retrograde (from the tip to the base of the cilium via dynein-2), which is dependent on the IFT-B and IFT-A complex, respectively. The IFT complexes are involved in the molecular transport in cilium (6).

CP110 and its interactor CEP97 are the key negative-regulators for cilium formation (7, 8). The CP110-CEP97 complex normally forms a cap at the distal end of centrioles to prevent microtubule growth in proliferating cells. Upon serum starvation, the CP110-CEP97 complex is specifically released from the mother centriole. Loss of either CEP97 or CP110 induces cilium formation even in serum-fed cells, whereas the overexpression of these proteins inhibits cilium formation in serum-starved cells (7).Primary cilia were never formed in T lymphocytes, but CP110 knockdown can produce the primary cilia (9). The specific removal of CP110-CEP97 from the mother centriole is crucial for cilium formation. Recent studies identified several proteins that are involved in this step. Tau tubulin kinase 2 (TTBK2) is a member of the casein kinase family and localizes to the tip of microtubules (10, 11). TTBK2 mutations cause the neurodegenerative disorder spinocerebellar ataxia type 11 (SCA11) and these mutants inhibit CP110 removal from the mother centriole and IFT recruitment to this site (12). After the formation of ciliary vesicles, TTBK2 accumulates to mother centriole through CEP164, C2CD3, and CEP350, and this accumulation triggers CP110 removal and IFT recruitment (12–16). Besides TTBK2, MARK4 is required for CP110 removal. Depletion of MARK4 induces mis-localization of ODF2 (MARK4 interactor) and inhibits CP110 removal from the mother centriole (17). MPP9 was identified as an interacting protein of CEP97 by proximity-dependent biotinylation (BioID) analysis of centrosome-cilium interface (18). Similar to CP110 and CEP97, MPP9 disappears from the distal end of the mother centriole upon serum starvation. In serum-depleted cells, MPP9 is phosphorylated by TTBK2 and degraded through ubiquitin-proteasome system on the mother centriole (19). CEP97 cooperatively inhibits cilium formation with CP110 and is thought to be a chaperon for CP110 stabilization (5). CEP97 specifically disappears from the mother centriole in quiescent cells similar to CP110. However, the mechanisms of CEP97 removal from the mother centriole and its function in CP110 removal and

cilium formation have not fully understood. Recently, Nagai et al. in our laboratory showed that CEP97 is degraded upon serum starvation by the ubiquitin-proteasome system (20). They identified the CUL3-RBX1-KCTD10 complex as the E3 ligase complex required for CEP97 ubiquitination and degradation in quiescent cells (20). The level of the phosphorylated form of CEP97 was increased by the treatment of MG-132, an inhibitor of proteasome, in serum-starved cells, suggesting that CEP97 phosphorylation is involved in its degradation (20). However, the mechanism regulating CEP97 degradation upon serum starvation remains elusive.

In this study, I identified 14-3-3 proteins as the KCTD10-binding proteins and showed that 14-3-3 proteins also bind to CEP97. As shown in most case, 14-3-3 protein bind to KCTD10 and CEP97 in a phosphorylation-dependent manner. I also showed that CEP97-KCTD10 interaction is increased by the inhibitor of protein phosphatase and blocked by dominant-negative form of 14-3-3-β, suggesting that 14-3-3 proteins serve as a linker to stimulate the interaction between CEP97 and KCTD10, dependent on their phosphorylation. The amount of CEP97 bound to 14-3-3-β was increased upon serum starvation. Furthermore, overexpression of a dominant-negative form of 14-3-3-β suppressed CEP97 ubiquitination, removal of CEP97 from the mother centriole, and ciliogenesis. These results strongly suggest that 14-3-3 proteins play a crucial role in CEP97 ubiquitination and degradation and consequent ciliogenesis by promoting its binding to KCTD10.

Results

Identification of 14-3-3 proteins as the KCTD10-binding proteins

To examine the mechanisms regulating KCTD10 localization and activity and CEP97 ubiquitination under serum-starved conditions, I searched the KCTD10-binding proteins by proteomic analysis using mass spectrometry in collaboration with Dr. S. Kanno (Tohoku University). HEK293T cell lines stably expressing FLAG-tagged KCTD10 were established, and the cell lysates of the cells cultured under serum-fed and -starved conditions were immunoprecipitated with anti-FLAG antibody. The co-precipitated proteins were eluted by FLAG peptide, separated by SDS-PAGE, and analyzed by silver staining (Fig. 1A). The protein bands that were predominantly detected in the serum-starved sample were digested and analyzed by mass spectrometry. Among them, several isoforms (β, ζ, θ) of 14-3-3 proteins were identified as the KCTD10-binding proteins (Fig. 1A).

To investigate the region of KCTD10 required for 14-3-3-β binding, HEK293T cells were transfected with YFP-tagged KCTD10 or its N- or C-terminal fragments (Fig. 1B), and cell lysates were subjected to pull-down assays with GST-14-3-3-β-conjugated beads. Immunoblot analyses with anti-GFP antibody revealed that the C-terminal fragment of KCTD10 binds to 14-3-3-β, but the binding of N-terminal fragment was barely detected (Fig. 1C), indicating that KCTD10 binds to 14-3-3-β through its C-terminal region.

CEP97 binds to 14-3-3-β

KCTD10 interacts with various centrosomal proteins, including CEP97, CEP76, and B9D1. To examine whether 14-3-3 proteins bind to these KCTD10-interactors, I analyzed their interactions by co-immunoprecipitation assays. HEK 293T cells were co-transfected with Myc-tagged wild-type (WT) 14-3-3-β and mCherry-tagged CEP97, CEP76 or B9D1. Cell lysates were immunoprecipitated with anti-mCherry nanobody beads and precipitates were analyzed by immunoblotting with anti-Myc and anti-mCherry antibodies. This analysis showed that CEP97, but neither CEP76 nor B9D1, strongly binds to 14-3-3-β (Fig. 2A).

CEP97 and KCTD10 bind to 14-3-3-β, dependent on their phosphorylation

It is well-known that 14-3-3 proteins associate with the proteins in a manner dependent on the phosphorylation of target proteins. The RA mutant of 14-3-3-β, in which Arg-48 and Arg-52 are replaced by alanine, can form a dimer with 14-3-3-β-WT, but cannot bind to the phosphorylated substrates and thereby act as a dominant negative form (Fig. 2B) (21). Co-precipitation assays showed that CEP97 binds to 14-3-3-β-WT but not to 14-3-3-β-RA, suggesting that CEP97 binds to 14-3-3-β in a manner dependent on CEP97 phosphorylation (Fig. 2A). To confirm this, I examined the effect of lambda protein phosphatase treatment on the 14-3-3-β-binding ability of CEP97. RPE1 cells were cultured for 48 hours and then treated with 0.3 μM MG-132, an inhibitor of proteasome, under serum-starved conditions for 24 h. Cell lysates were treated with lambda phosphatase for 1 h and then subjected to GST-14-3-3-β pull down assays. CEP97 was pulled-down with GST-14-3-3-β without lambda phosphatase treatment but it was not pulled down after treatment with lambda phosphatase (Fig. 2C), indicating that CEP97 binds 14-3-3-β to in a phosphorylation-dependent manner. Similarly, the amount of KCTD10 that was pulled-down with GST-14-3-3-β was dramatically reduced after treatment with lambda phosphatase, suggesting that KCTD10 also bind to 14-3-3-β in a phosphorylation-dependent manner.

CEP97 ubiquitination is promoted by phosphorylation

As previously reported (20), the level of CEP97 protein was decreased upon serum starvation and the level of phosphorylated CEP97 increased after the treatment with MG-132 under serum-starved conditions (Fig. 3A). These results suggest that CEP97 phosphorylation is involved in its ubiquitination and degradation. To examine the role of CEP97 phosphorylation in its ubiquitination, I analyzed the effect of inhibitors of protein kinases and phosphatases on CEP97 ubiquitination. RPE1 cells were cultured for 48 h and treated with 0.3 μM MG-132 for 24 h under serum-starved conditions in the presence or absence of the inhibitors of protein kinases or phosphatase. To collect ubiquitinated CEP97 proteins, I used GST-tagged tandem-repeated ubiquitin-binding entities (TUBEs) that consist of four ubiquitin-associated domains and effectively bind to poly-ubiquitinated proteins (22). Cell lysates were pulled-down with GST-tagged TUBEs-conjugated beads and the precipitates were subjected to SDS-PAGE and analyzed by immunoblotting with anti-CEP97 and anti-ubiquitin antibodies. The level of ubiquitinated CEP97 was decreased by the treatment with staurosporine, a general inhibitor of protein kinases but increased by the treatment with okadaic acid (OA), an inhibitor of protein phosphatase PP2A, in serum-starved cells (Fig. 3B and 3C). These results indicate that CEP97 ubiquitination is promoted by its phosphorylation.

The CEP97-KCTD10 interaction depends on phosphorylation

To investigate whether the interaction between CEP97 and KCTD10 depends on phosphorylation, I examined the effect of OA treatment on their interaction. RPE1 cells stably expressing YFP-tagged KCTD10 were treated with 0.3 μM MG-132 for 24 h under serum-starved conditions in the presence or absence of OA, and cell lysates were immunoprecipitated with anti-GFP nanobody beads. The co-precipitates were analyzed by immunoblotting with anti-CEP97 and anti-GFP antibodies. Treatment with OA markedly increased the amount of CEP97 that was bound to KCTD10 (Fig. 3D), indicating that the CEP97-KCTD10 interaction is promoted by the phosphorylation of CEP97 and/or KCTD10. Additionally, OA treatment increased the amount of CUL3 that was bound to KCTD10 in serum-starved and MG-132-treated RPE1 cells (Fig. 3D), indicating that the interaction between KCTD10 and CUL3 also depends on the phosphorylation state of KCTD10 and/or CUL3.

Serum starvation promotes the interaction between CEP97 and 14-3-3-β

Next, I examined whether the interaction between CEP97 and 14-3-3-β is regulated by serum starvation by GST-14-3-3-β pull-down assay. RPE1 cells were cultured for 48 h and then treated with 0.3 μM MG-132 in the presence or absence of serum for 24 h. Cell lysates were pulled-down with GST-tagged 14-3-3-β and the precipitates were analyzed by immunoblotting with anti-CEP97 antibody. This assay showed that the amount of CEP97 that was bound to 14-3-3-β was increased under serum-starved conditions, compared to that under serum-supplemented conditions (Fig. 3E). These results suggest that serum starvation induces the binding of CEP97 to 14-3-3-β.

Dominant-negative 14-3-3-β blocks the CEP97-KCTD10 interaction and CEP97 ubiquitination

14-3-3 isoforms form homo- and hetero- dimers with each isoform. In terms of 14-3-3-β, 14-3-3-β can bind to β and γ (23). To confirm this, I examine the interaction between 14-3-3-β and each isoform. HEK293T cells were transfected with Myc-tagged GFP or 14-3-3 isoforms. Cell lysates were pulled-down with GST-14-3-3-β conjugated beads and the precipitates were analyzed by immunoblotting with an anti-Myc antibody. Pull-down assay revealed that each of 14-3-3 isoforms interacts with 14-3-3-β (Fig. S1). To investigate the role of 14-3-3-β in the CEP97-KCTD10 interaction, I next analyzed that the effect of overexpression of the dominant-negative form of 14-3-3-β (14-3-3-β-RA)

on the CEP97-KCTD10 interaction. HEK293T cells were co-transfected with Myc-tagged 14-3-3-β-(WT or -RA), mCherry-tagged CEP97, and FLAG-tagged KCTD10. Cell lysates were immunoprecipitated with anti-mCherry nanobody conjugated beads and the precipitates were analyzed by immunoblotting with anti-FLAG and anti-mCherry antibodies. Co-precipitation assays revealed that KCTD10 was co-precipitated with CEP97 (Fig. 4A), as reported (20). Intriguingly, co-expression of 14-3-3-β-RA markedly suppressed the binding of CEP97 to KCTD10, whereas co-expression of 14-3-3-β-WT had no apparent effect on their interaction between CEP97 and KCTD10 (Fig. 4A). These results indicate that 14-3-3-β is involved in the interaction between CEP97 and KCTD10.

To investigate the role of 14-3-3-β in serum-starved-induced CEP97 ubiquitination, I analyzed the effect of overexpression of 14-3-3-β-RA on the level of CEP97 ubiquitination. HEK293T cells were co-transfected with mCherry-tagged CEP97 and Myc-tagged 14-3-3-β-(WT or -RA) and cultured for 24 h in serum-starved medium with 0.3 μM MG-132. Cell lysates were pulled-down with GST-TUBEs to collect ubiquitinated proteins, and precipitates were analyzed by immunoblotting with anti-mCherry antibody to detect ubiquitinated CEP97-mCherry. This analysis showed that co-expression of dominant-negative 14-3-3-β-RA substantially reduced the level of CEP97 ubiquitination in serum-starved cells (Fig. 4B). These results suggest that 14-3-3-β plays a crucial role in CEP97 ubiquitination in serum-starved cells, probably through promoting the binding of CEP97 to KCTD10.

I also examined the effects of expression of 14-3-3-β-(WT or -RA) on the ubiquitination of the centrosomal proteins CEP76 and MPP9. MPP9 is known to be ubiquitinated upon serum starvation (19). In contrast to the effect on CEP97 ubiquitination, overexpression of 14-3-3-β-RA had no apparent effect on the ubiquitination of CEP76 or MPP9 (Fig. 4C).

Expression of dominant-negative 14-3-3-β impairs CEP97 removal and ciliogenesis

Next, I analyzed the effects of overexpression of 14-3-3-β-(WT or -RA) on serum-starvation-induced ciliogenesis. RPE1 cells were transfected with GFP or GFP-tagged 14-3-3-β-(WT or -RA), serum-starved for 48 h, and stained with antibodies against anti-g-tubulin (as a marker of the centrosome), and acetylated-tubulin (as a marker of ciliary axoneme) (Fig. 5A). Whereas primary cilia were formed in 57% of control GFP cells, overexpression of 14-3-3-β-RA significantly reduced the percentages of ciliated cells to 16% (Fig. 5A and 5B). Overexpression of 14-3-3-β-WT slightly reduced the percentages of ciliated cells to 39% (Fig. 5A and 5B), and it might be due to the effect that the overexpression of 14-3-3-b promotes proliferation as previously reported (24). These results suggest that 14-3-3-β plays a crucial role in ciliogenesis.

CEP97 is removed from the mother centriole upon serum starvation but remains localization to the daughter centriole in ciliated cells (7). I next examined the effect of overexpression of 14-3-3-β-(WT or -RA) on CEP97 removal from the mother centriole after serum starvation. RPE1 cells were transfected with GFP or GFP-tagged 14-3-3-β-(WT or -RA), serum-starved for 48 h, and stained with antibodies against anti-FOP (as a marker of the centrioles), and CEP170 (as a marker of mother centriole) (Fig. 5C). In most of control GFP-expressing cells, CEP97 was localized to a single centriole, indicating that CEP97 had been removed from the mother centriole upon serum starvation (Fig. 5C and 5D). Overexpression of 14-3-3-β-RA decreased the population of cells with CEP97 localized to a single centriole and inversely increased the population of cells with CEP97 localized to two centrioles (Fig. 5C and 5D). Quantitative analyses showed that the population of cells with CEP97 localized to one centriole was 80% in control GFP-expressing cells, but it was decreased to 28% by overexpression of 14-3-3-β-RA (Fig. 5D). Overexpression of 14-3-3-β-WT modestly reduced the population of cells with CEP97 localized to a single centriole (Fig. 5C and 5D). These results suggest that expression of

dominant-negative form of 14-3-3-β severely suppresses the removal of CEP97 from the mother centriole and that 14-3-3-β plays a critical role in serum-starvation-induced CEP97 removal from the mother centriole for initiating ciliogenesis.

Discussion

The CP110-CEP97 complex cooperatively inhibits abnormal ciliogenesis in cycling cells (7). CP110 and CEP97 are specifically removed from the mother centriole in quiescent cells and this removal initiates axoneme elongation and ciliogenesis. Our group recently showed that CEP97 is degraded in quiescent cells by the ubiquitin-proteasome system using the KCTD10-RBX1-CUL3 complex as the E3 ubiquitin ligase, but the precise mechanism of the serum-starvation-induced CEP97 degradation remains to be solved. In this study, I identified 14-3-3 proteins as the KCTD10-ineteractors. 14-3-3 proteins also interact with CEP97 in a phosphorylation-dependent manner. The amount of CEP97 that was bound to 14-3-3-β was increased upon serum starvation. My results in this study strongly suggest that the phosphorylation of CEP97 and its binding to 14-3-3 proteins play crucial roles in CEP97 removal from the mother centriole and degradation upon serum starvation (Fig. 6).

Previous studies have shown that several isoforms of 14-3-3 proteins are localized to the centrosome and removed from the centrosome upon serum-starvation (25). This observation is consistent with CEP97 removal from the mother centriole. The ubiquitination assays using TUBEs showed that 14-3-3-β-WT, but not its RA mutant, is ubiquitinated in serum-starved cells. These results suggest that 14-3-3-β bound to CEP97 is ubiquitinated and removed from the mother centriole, together with CEP97. Another report showed that 14-3-3-η localizes to the cell junctions and primary cilia and depletion of 14-3-3-η suppresses ciliogenesis in MDCK cells, co-operatively with two cell polarity complex, the aPKC/Par complex and the CRB3/PATJ1/PALS complex (26). This observation is also consistent with my observation that the overexpression of the dominant-negative form of 14-3-3-β blocked CEP97 removal from the mother centriole and ciliogenesis. Furthermore, depletion of some 14-3-3 isoforms in mice caused hydrocephalus and reduction of cilium formation in ependymal cells (personal communication from Dr. S. Ohata, Musashino University). These results further support the crucial role of 14-3-3 proteins in ciliogenesis. Analyses of CEP97 localization and the effects of CEP97 knockdown on cilium formation in 14-3-3 KO cells, will further clarify the importance of 14-3-3-CEP97 interaction in ciliogenesis.

14-3-3 proteins form homo- or hetero-dimers and engage the phosphorylation-dependent interactions between a wide range of client proteins. Binding of 14-3-3 proteins promotes and inhibits specific protein–protein interactions, dependent on the situations, resulting in modulation of enzymatic activity and sequestration of binding partners away from their normal sites of action (27). In fact, this study showed that CEP97 interacts with 14-3-3 protein in a phosphorylation-dependent manner and this interaction promotes the association of CEP97 with KCTD10. Previous studies showed that 14-3-3 proteins bind to target proteins through the consensus motif, R-X-X-S(P), where S(P) is the phosphorylated serine residue (28). CEP97 has no such sequence motif. KCTD10 has the sequence of RTTS in the N-terminal region (amino acids 20-23), but S23A mutant of KCTD10 also binds to 14-3-3-β (data not shown). Further studies are required to identify the residues responsible for the phosphorylation-dependent binding to 14-3-3 proteins.

CP110 and MPP9 interacts with CEP97 and these three proteins are co-operatively removed from the mother centriole during ciliogenesis through the ubiquitin-proteasome system (19, 20, 29). Overexpression of 14-3-3-β-RA had no apparent effect on the ubiquitination of CP110 and MPP9 in quiescent cells, suggesting that 14-3-3 proteins are specifically involved in the ubiquitination of CEP97 during cilium formation. In this research, I found that CEP97 phosphorylation is involved in its ubiquitination. However, the protein kinases that are involved in the phosphorylation of CEP97 in serum-starved cells remain unknown. MPP9 is removed from the mother centriole by TTBK2-mediated phosphorylation and subsequent ubiquitination and degradation (19). MARK4 accumulates at the basal body and is

required for CP110 removal (17). Preliminary studies showed that TTBK2 has the ability to phosphorylate CEP97 in vitro kinase assays but depletion of TTBK2 has no apparent effect on CEP97 phosphorylation in serum-starved cells (15) (data not shown), indicating that the protein kinases other than TTBK2 is involved in the serum-starvation-induced CEP97 phosphorylation.

I also showed that KCTD10 interacts with 14-3-3-β in a phosphorylation-dependent manner. Although the role of KCTD10 phosphorylation remains unclear, the OA treatment promoted the binding of KCTD10 to CEP97 and CUL3, indicating that these interactions are increased by KCTD10 phosphorylation. A previous study showed that the activities of some of the E3 ubiquitin ligases are increased by their phosphorylation (30). Future studies will reveal the role of the phosphorylation of KCTD10 in CEP97 degradation and cilium formation.

Materials and Methods

Cell culture

Human telomerase reverse transcriptase-immortalized retinal pigmented epithelial (RPE)-1 cells were provided by Hiroyuki Nakanishi (Kumamoto University). Cells had recently been authenticated and tested for contamination. RPE1 cells were cultured in Dulbecco's modified Eagle's medium (DMEM)/Ham's F-12 (042-30555; Wako Pure Chemical) supplemented with 10% fetal bovine serum (FBS; Biosera). HEK293T cells were obtained from ATCC (No. CRL-3216) were cultured in DMEM (044-29765; Wako Pure Chemical) supplemented with 10% FCS. Both cell lines were tested for mycoplasma contamination and found to be negative. RPE1 cells were transiently transfected with plasmid DNA using Lipofectamine LTX with PLUS reagent (Thermo Fisher Scientific). HEK293T cells were transfected with plasmid DNA using JetPEI (PolyPlus).

Reagents and antibodies

MG-132 (C2211; Millipore Sigma), 4′,6-diamidino-2- phenylindole (DAPI) (09224; Polysciences), Okadaic acid (10011490, Cayman Chemical Company) were purchased from indicated suppliers. Rabbit polyclonal antibodies against CEP97 (NBP1-83591, Novus Biologicals), KCTD10 (Novus Biologicals), CUL3 (2759S, Cell signaling), c- Myc (562; Medical and Biological Laboratories), mCherry (GTX128508, Gene Tex) and GFP (A6455, Molecular Probes) were purchased from the specified suppliers. Mouse monoclonal antibodies against c-Myc (PL14, Medical and Biological Laboratories), FLAG (F1804, Millipore Sigma), Ubiquitin FK2 (BML-PW8810, Enzo), α-tubulin (T6074, Millipore Sigma) , γ-tubulin (T5326, Millipore Sigma), acetylated (Ac)-tubulin (T6793, Millipore Sigma), FOP (H00011116-M01, Abnova), and CEP170 (72-413-1, Thermo Fisher Scientific) were purchased from the specified suppliers. Secondary antibodies conjugated with horseradish peroxidase (HRP) against mouse IgG (NA931, GE Healthcare) and rabbit IgG (NA934, GE Healthcare) were purchased from the suppliers indicated. Secondary antibodies conjugated with Alexa Fluor 488 against mouse IgG (A11029) and rabbit IgG (A11034), those with Alexa Fluor 568 against mouse IgG (A11031), Alexa Fluor 350 against mouse IgG2b (A21140), Alexa Fluor 647 against mouse IgG1 (A21240), and Alexa Fluor 633 against mouse IgG (A21052) were purchased from Life Technologies.

Plasmid construction

Human cDNAs for CEP97 and CP110 were provided by Tetsuo Kobayashi (Nara Institute of Science and Technology) and Brian D. Dynlacht (New York University). Human cDNAs for KCTD10 was provided by Naoki Goshima (National Institute of Advanced Industrial Science and Technology). Human cDNAs for 14-3-3 isoforms were PCR-amplified from a megaman human transcriptome library (Agilent) and subcloned into pcDNA-Myc+His vector. Fragments of KCTD10 and CEP97 were constructed by site-directed PCR. Human cDNA for CEP76, MPP9, and B9D1 were PCR-amplified from a megaman human transcriptome library (Agilent).

Immunoprecipitation and nanoLC/MS/MS

The HEK293 cells stably expressing Flag-KCTD10 by Flip-in T-Rex system (1 ml) and the control cells (induced pcDNA5/FRT/TO vector only) (1 ml) were homogenized in SHE buffer (10 mM HEPES (pH 7.4), 0.21 M mannitol, 0.07 M sucrose, 0.1 M EDTA, 0.1 M EGTA, 0.15 mM spermine, 0.75 mM spermidine) and centrifuged for 10 min at 3000 rpm. The pellets were rinsed with SHE buffer and centrifuged once more. The pellets were then extracted in

1 ml of extraction buffer (50mM HEPES pH 7.4, 0.3M NaCl, 0.2% NP-40) by sonication and the extracts were clarified by centrifugation at 12 000 rpm. for 30 min at 4°C.The nuclear extracts were incubated with anti-flag antibody M2 beads for 4 h in the presence of RNase A (10mg/ml) and DNase I (10mg/ml) at 4˚C, After washing three times with washing buffer (0.15M NaCl. 0.1% NP-40, 50 mM HEPES pH 7.4) and once with PBS, the binding proteins were eluted by 40□l of 0.1M glycine buffer pH 3.0. The elutes were neutralized by 1M Tris-HCl buffer pH 9.5 and suspended in SDS-PAGE sample buffer. The samples were boiled for 5min and were resolved by SDS-PAGE. The gel was stained using a Wako Mass silver stain kit. Gel slippage was reduced by 100 mM of DTT and alkylated by 100 mM idoacetamide. After washing, the gels were incubated with trypsin overnight at 30°C. Recovered peptides were desalted by Ziptip c18 (Millipore). Samples were analyzed by nanoLC/MS/MS systems (DiNa HPLC system KYA TECH Corporation/QSTAR XL Applied Biosystems). Mass data acquisitions were piloted by Mascot software.

Conjugation of GST-fusion proteins to glutathione-Sepharose beads

GST-fusion proteins (GST-anti-GFP nanobody, GST-anti-mCherry nanobody, GST-TUBEs, and GST-14-3-3-β) were expressed in *Escherichia coli* (*E.coli*) BL-21 cells. Cells were cultured in 5 ml of ampicillin-containing 2xYT medium for overnight at 37°C and transferred to 200 ml of 2x YT medium. After culturing cells for 1 h at 37°C, isopropyl β-D-thiogalactopyranoside (IPTG) was added to the culture and incubated for overnight at 18°C. Cells were lysed with lysis buffer (50 mM Tris-HCl pH 7.4, 150 mM NaCl, 1% TritonX-100, 5% glycerol, 1 mM dithiothreitol (DTT), 1 mM PMSF, and 1 mM EGTA). Cell lysates were incubated with glutathione-Sepharose 4B (GE Healthcare).

Immunoprecipitation and pull-down assay

Cells were lysed with lysis buffer (150 mM NaCl, 20 mM HEPES-KOH, pH 7.4, 1% Triton X-100, 5% glycerol, 1 mM Na_3VO_4, 10 μg/mL leupeptin, 3 μg/mL pepstatin, and 1 mM DTT) and centrifuged. Lysates were pre-cleared with Protein A-Sepharose (GE Healthcare) for 1 h at 4°C, and the supernatants were incubated with GST-anti-mCherry-nanobody, GST-anti-GFP-nanobody, or GST-14-3-3-β pre-bound to glutathione-Sepharose beads for 4 h or overnight at 4°C. To examine whether CEP97 phosphorylation is involved in 14-3-3-β interaction, MG-132- treated cell lysates were incubated with 0.25 U/μl of λ-phosphatase (New England BioLabs) for 2 hours prior to pull-down assay. After centrifugation, precipitates were washed three times and used for the immunoblot analyses.

Collection of ubiquitinated protein

Cells were lysed with lysis buffer (150 mM NaCl, 20 mM HEPES-KOH, pH 7.4, 1% Triton X-100, 5% glycerol, 20 mM N-ethylmaleimide, 1 mM Na_3VO_4, 10 μg/mL leupeptin, 3 μg/mL pepstatin, and 1 mM DTT) and centrifuged. Lysates were pre-cleared with Protein A-Sepharose (GE Healthcare) for 1 h at 4°C, and the supernatants were incubated with GST-TR-TUBE pre-bound to glutathione-Sepharose beads (GE Healthcare) for overnight at 4°C. After centrifugation, precipitates were washed three times and used for the immunoblot analysis.

Immunoblotting

Samples were separated by SDS-PAGE and transferred onto Immobilon-P polyvinylidene difluoride membranes (Millipore). The membranes were blocked with 5% non-fat dry milk in PBS- T. The membranes were incubated with the primary antibodies for 1.5 h at room temperature or overnight at 4°C. After washing the membranes three times with PBS-T, they were incubated with HRP-conjugated secondary antibody for 1.5 h. After washing, the

membranes were reacted with Immobilon Western (Millipore) and the immunoreactive protein bands were visualized using a ChemiDoc Touch Imaging System (Bio-Rad). Images were analyzed by using ImageJ.

Immunostaining and fluorescence microscopy

Cells were fixed with 4% paraformaldehyde at room temperature for 30 min, washed twice with PBS for 5 min, and then permeabilized by treatment with methanol for 10 min at -20°C. After two washes with PBS, the cells were blocked with 2% FBS in PBS for 30 min at room temperature and incubated with the appropriate primary antibodies overnight at 4°C. After washing with PBS three times, the cells were incubated with Alexa-568-, Alexa-633-conjugated secondary antibodies in PBS containing 2% FBS for 1.5 h. Nuclear DNA was stained with DAPI. Fluorescence images were obtained using a fluorescence microscopy (DMi8, Leica Microsystems), equipped with a 100x oil immersion objective lens (NA 1.3) and a CMOS camera (C13440-20CU; Hamamatsu Photonics) driven by LAS AF Imaging Software (Leica Microsystems). Images were analyzed by using ImageJ.

Statistical analyses

Statistical analysis included one-way analysis of variance (ANOVA) followed by Dunnett's test for comparison of multiple data sets and was performed using Prism software version 6.0 c (GraphPad Software). Data represent the means of the indicated number of independent experiments. Error bars indicate the standard error of the mean (S.E.M.). Statistical significance was set at $p < 0.05$.

References

1. Goetz, S. C., and Anderson, K. V (2010) The primary cilium: A signalling centre during vertebrate development. *Nat. Rev. Genet.* **11**, 331–344
2. Friedhelm, H., Thomas, B., and Katsanis, N. (2011) Ciliopathies. *N. Engl. J. Med.*
3. Izawa, I., Goto, H., Kasahara, K., and Inagaki, M. (2015) Current topics of functional links between primary cilia and cell cycle. *Cilia*. **4**, 1–13
4. Sorokin, S., 1962 (1962) Centrioles and the formation of rudimentary cilia by fibroblasts and smooth muscle cells. *J. Cell Biol.* **15**, 363–377
5. Kobayashi, T., and Dynlacht, B. D. (2011) Regulating the transition from centriole to basal body. *J. Cell Biol.* **193**, 435–444
6. Ishikawa, H., and Marshall, W. F. (2017) Intraflagellar transport and ciliary dynamics. *Cold Spring Harb. Perspect. Biol.* 10.1101/cshperspect.a021998
7. Spektor, A., Tsang, W. Y., Khoo, D., and Dynlacht, B. D. (2007) Cep97 and CP110 Suppress a Cilia Assembly Program. *Cell*. **130**, 678–690
8. Tsang, W. Y., and Dynlacht, B. D. (2013) CP110 and its network of partners coordinately regulate cilia assembly. *Cilia*. **2**, 2–9
9. Prosser, S. L., and Morrison, C. G. (2015) Centrin2 regulates CP110 removal in primary cilium formation. *J. Cell Biol.* **208**, 693–701
10. Takahashi, M., Tomizawa, K., Sato, K., Ohtake, A., and Omori, A. (1995) A novel tau-tubulin kinase from bovine brain. *FEBS Lett.* **372**, 59–64
11. Watanabe, T., Kakeno, M., Matsui, T., Sugiyama, I., Arimura, N., Matsuzawa, K., Shirahige, A., Ishidate, F., Nishioka, T., Taya, S., Hoshino, M., and Kaibuchi, K. (2015) TTBK2 with EB1/3 regulates microtubule dynamics in migrating cells through KIF2A phosphorylation. *J. Cell Biol.* **210**, 737–751
12. Goetz, S. C., Liem, K. F., and Anderson, K. V (2012) The spinocerebellar ataxia-associated gene tau tubulin kinase 2 controls the initiation of ciliogenesis. *Cell*. **151**, 847–858
13. Ye, X., Zeng, H., Ning, G., Reiter, J. F., and Liu, A. (2014) C2cd3 is critical for centriolar distal appendage assembly and ciliary vesicle docking in mammals. *Proc. Natl. Acad. Sci.* **111**, 2164–2169
14. Kanie, T., Abbott, K. L., Mooney, N. A., Plowey, E. D., Demeter, J., and Jackson, P. K. (2017) The CEP19-RABL2 GTPase Complex Binds IFT-B to Initiate Intraflagellar Transport at the Ciliary Base. *Dev. Cell*. **42**, 22-36.e12
15. Oda, T., Chiba, S., Nagai, T., and Mizuno, K. (2014) Binding to Cep164, but not EB1, is essential for centriolar localization of TTBK2 and its function in ciliogenesis. *Genes to Cells*. **19**, 927–940
16. Cajanek, L., and Nigg, E. A. (2014) Cep164 triggers ciliogenesis by recruiting Tau tubulin kinase 2 to the mother centriole. *Proc. Natl. Acad. Sci.* **111**, E2841–E2850
17. Kuhns, S., Schmidt, K. N., Reymann, J., Gilbert, D. F., Neuner, A., Hub, B., Carvalho, R., Wiedemann, P., Zentgraf, H., Erfle, H., Klingmüller, U., Boutros, M., and Pereira, G. (2013) The microtubule affinity regulating kinase MARK4 promotes axoneme extension during early ciliogenesis. *J. Cell Biol.* **200**, 505–522
18. Gupta, G. D., Coyaud, É., Gonçalves, J., Mojarad, B. A., Liu, Y., Wu, Q., Gheiratmand, L., Comartin, D., Tkach, J. M., Cheung, S. W. T., Bashkurov, M., Hasegan, M., Knight, J. D., Lin, Z. Y., Schueler, M.,

Hildebrandt, F., Moffat, J., Gingras, A. C., Raught, B., and Pelletier, L. (2015) A Dynamic Protein Interaction Landscape of the Human Centrosome-Cilium Interface. *Cell*. **163**, 1483–1499

19. Huang, N., Zhang, D., Li, F., Chai, P., Wang, S., Teng, J., and Chen, J. (2018) M-Phase Phosphoprotein 9 regulates ciliogenesis by modulating CP110-CEP97 complex localization at the mother centriole. *Nat. Commun.* **9**, 4511
20. Nagai, T., Mukoyama, S., Kagiwada, H., Goshima, N., and Mizuno, K. (2018) Cullin-3-KCTD10-mediated CEP97 degradation promotes primary cilium formation. *J. Cell Sci.* 10.1242/jcs.219527
21. Thorson, J. A., Yu, L. W. K., Hsu, A. L., Shih, N.-Y., Graves, P. R., Tanner, J. W., Allen, P. M., Piwnica-Worms, H., and Shaw, A. S. (1998) 14-3-3 Proteins are required for maintenance of Raf-1 phosphorylation and kinase activity. *Mol. Cell. Biol.* **18**, 5229–5238
22. Hjerpe, R., Aillet, F., Lopitz-Otsoa, F., Lang, V., England, P., and Rodriguez, M. S. (2009) Efficient protection and isolation of ubiquitylated proteins using tandem ubiquitin-binding entities. *EMBO Rep.* **10**, 1250–1258
23. Aitken, A. (2002) Functional specificity in 14-3-3 isoform interactions through dimer formation and phosphorylation. Chromosome location of mammalian isoforms and variants. *Plant Mol. Biol.* **50**, 993–1010
24. Gong, F., Wang, G., Ye, J., Li, T., Bai, H., and Wang, W. (2013) 14-3-3β regulates the proliferation of glioma cells through the GSK3β/β-catenin signaling pathway. *Oncol. Rep.* **30**, 2976–2982
25. Pietromonaco, S. F., Seluja, G. A., Aitken, A., and Elias, L. (1996) Association of 14-3-3 proteins with centrosomes. *Blood Cells, Mol. Dis.* **22**, 225–237
26. Fan, S., Hurd, T. W., Liu, C.-J., Straight, S. W., Weimbs, T., Hurd, E. A., Domino, S. E., and Ben Margolis (2004) Polarity proteins control ciliogenesis via kinesin motor interactions. *Curr. Biol.* **14**, 1451–1461
27. Ichimura, T., Taoka, M., Shoji, I., Kato, H., Sato, T., Hatakeyama, S., Isobe, T., and Hachiya, N. (2013) 14-3-3 proteins sequester a pool of soluble TRIM32 ubiquitin ligase to repress autoubiquitylation and cytoplasmic body formation. *J. Cell Sci.* **126**, 2014–2026
28. Obsil, T., and Obsilova, V. (2011) Structural basis of 14-3-3 protein functions. *Semin. Cell Dev. Biol.* **22**, 663–672
29. Loukil, A., Tormanen, K., and Sütterlin, C. (2017) The daughter centriole controls ciliogenesis by regulating Neurl-4 localization at the centrosome. *J. Cell Biol.* **216**, 1287–1300
30. Lewandowski, K. T., and Piwnica-Worms, H. (2014) Phosphorylation of the E3 ubiquitin ligase RNF41 by the kinase Par-1b is required for epithelial cell polarity. *J. Cell Sci.* **127**, 315–327

Figure Legends

Fig. 1. Identification of 14-3-3 proteins as the KCTD10 interactors.

(A) Identification of KCTD10-binding proteins. HEK293T cell lines stably expressing FLAG-KCTD10 were established. cells were cultured under serum-fed or -starved conditions, and cell lysates were immunoprecipitated with anti-FLAG antibody. The precipitated proteins were eluted with FLAG peptide, separated by SDS-PAGE and stained by silver. The proteins were identified by mass spectrometric analyses.

(B) Schematic structures of full-length (FL) KCTD10 and its N- and C-terminal fragments.

(C) Pull-down assays using GST-14-3-3-β. HEK293T cells were transfected with YFP-tagged KCTD10-FL or its deletion mutants and cell lysates pulled-down with GST or GST-14-3-3-β. Precipitates and cell lysates were analyzed by immunoblotting with anti-GFP antibody. GST and GST-14-3-3-β were analyzed by amido black staining.

Fig.2 CEP97 interacts with 14-3-3-β in a phosphorylation-dependent manner.

(A) CEP97 binds to 14-3-3-β. HEK293T cells were co-transfected with Myc-14-3-3-β and mCherry-tagged CEP97, CEP76 or B9D1. Cell lysates were immunoprecipitated with anti-mCherry nanobody beads. Beads and lysates were analyzed by immunoblotting with anti-Myc and anti-mCherry antibodies.

(B) Illustration of 14-3-3-β-WT and its dominant-negative RA mutant, in which Arg-48 and Arg-52 were replaced by alanine. The RA mutant can form a dimer with 14-3-3-β-WT but cannot bind to the phosphorylated proteins, and thereby it acts as a dominant-negative form.

(C) CEP97 and KCTD10 interact with 14-3-3-β in a phosphorylation-dependent manner. RPE1 cells were serum-starved in the presence of 0.3 μM MG-132. Cell lysates were treated with lambda protein phosphatase (λPP) or untreated and then subjected to pull-down assays with GST-14-3-3-β, as in Fig. 1C.

Fig. 3. CEP97 interacts with 14-3-3-β upon serum starvation.

(A) Changes in the levels of CEP97 upon serum starvation and effect of MG-132 treatment. RPE1 cells were serum-starved for 24 h and then treated with DMSO or 0.3 μM MG-132 in the 0.2% serum-containing medium for 24 h. Cell lysates were analyzed by immunoblotting with anti-CEP97 and anti-α-tubulin antibodies.

(B) Effect of staurosporine on CEP97 ubiquitination under serum-starved conditions. RPE1 cells were serum-starved with 0.3 μM MG-132 and 2 μM staurosporine for 24 hours. Ubiquitinated proteins were collected using GST-TUBEs conjugated beads from cell lysates. Samples were analyzed by immunoblotting using anti-CEP97 and anti-ubiquitin antibodies.

(C) Effect of okadaic acid (OA) on CEP97 ubiquitination. RPE1 cells were serum-starved with 0.3 μM MG-132 for 24 hours and treated with 100 nM OA in the medium containing 0.2% FBS and 0.3 μM MG-132 for 1 hour. Ubiquitinated proteins were collected using GST-TUBE conjugated beads from cell lysates. Samples were analyzed by immunoblotting using anti-CEP97 and anti-ubiquitin antibodies.

(D) OA promotes KCTD10-CEP97 interaction and KCTD10-CUL3 interaction. YFP tagged KCTD10 stably expressing RPE1 cells were serum-starved with 0.3 μM MG-132 for 24 h and treated with 100 nM OA in the medium containing 0.2% FBS and 0.3 μM MG-132 for 1 hour. Cell lysates were immunoprecipitated with anti-GFP nanobody conjugated beads and precipitates were immunoblotted using anti-CUL3, anti-CEP97, and anti-GFP antibodies.

(E) 14-3-3-β strongly binds to CEP97 during serum starvation. RPE1 cells were cultured with or without serum for 24 h.

Cell lysates were pulled-down with GST-14-3-3-β conjugated beads and samples were analyzed by immunoblotting using anti-CEP97 antibody.

Fig.4 Dominant-negative 14-3-3-β inhibits CEP97 ubiquitination.

(A) Dominant-negative 14-3-3-β inhibits KCTD10-CEP97 interaction. Cell lysates from HEK293T cells expressing mCherry-CEP97, FLAG-KCTD10 and Myc-14-3-3-β WT/RA (dominant negative) were pulled-down with anti-mCherry nanobody and subjected to immunoblotting.

(B) Dominant-negative 14-3-3-β inhibits CEP97 ubiquitination during serum starvation. Cells were treated with 0.3 μM MG-132 in 0.2% FBS containing medium for 24 hours. Cell lysates were pull-downed with TUBEs conjugated beads.

(C) Dominant-negative 14-3-3 does not inhibit the ubiquitination of CEP76 and MPP9 during serum starvation. HEK293T cells expressing with Myc-tagged 14-3-3-β-(WT/-RA) and mCherry-tagged CEP76/MPP9 were treated with 0.3 μM MG-132 in 0.2% FBS containing medium for 24 hours. Cell lysates were pull-downed with TUBEs conjugated beads.

Fig.5 Dominant negative 14-3-3-β inhibits ciliogenesis and CEP97 removal.

(A) Overexpression of 14-3-3-β-RA blocks ciliogenesis in serum-starved cells. RPE1 cells were transfected with GFP or GFP-14-3-3-β-(WT/-RA) and serum-starved for 48 h. Cells were fixed and stained with anti-Ac-tubulin and anti-γ-tubulin (magenta) antibodies. Cells were also imaged by GFP fluorescence (green). Right panels show magnified images of the white boxes. Scale bars: 20 μm.

(B) Quantification of the percentage of ciliated cells based on staining with Ac-tubulin.

(C) Overexpression of 14-3-3-β-RA causes retention of CEP97 on the mother centrosome in serum-starved cells. RPE1 cells were transfected with GFP or GFP-14-3-3-β-(WT/-RA) and serum-starved for 48 h. Cells were fixed and stained with anti-CEP97 (green), anti-FOP (magenta) and anti-CEP170 (red) antibodies. Cells were also imaged by GFP fluorescence (blue). Right panels show magnified images of the white boxes. Arrow heads indicate the place of the mother centriole. Scale bars: 20 μm.

(D) Quantification of the percentage of cells categorized into one dot (CEP97 localization on one centriole) and two dots (CEP97 localization on two centriole). Data in (B) and (D) are presented as the mean±s.e.m. from three independent experiments with >100 cells per experiment. Statistical significance was calculated using ordinary one-way ANOVAs with Dunnett's test. n.s., not significant; *P<0.05; ***P<0.001.

Fig.6 A proposed model of the role of 14-3-3-β in CEP97 degradation.

Upon serum starvation, 14-3-3 proteins interact with phosphorylated CEP97 and KCTD10 and promotes their interaction. Then, CEP97 is ubiquitinated by the CUL3-RBX1-KCTD10 E3 ubiquitin ligase complex and degraded by ubiquitin-proteasome system. CEP97 degradation leads to CP110 destabilization and removal from the mother centriole and, thereby, induces axoneme extension to form the primary cilium. 97 and 110 indicate CEP97 and CP110, respectively. Ub, ubiquitin.

Fig. S1 14-3-3-β interacts with all of each isoform

Cell lysates from HEK293T cells expressing Myc-tagged GFP or 14-3-3 isoforms were pulled-down with GST-14-3-3-β conjugated beads and subjected to immunoblotting.

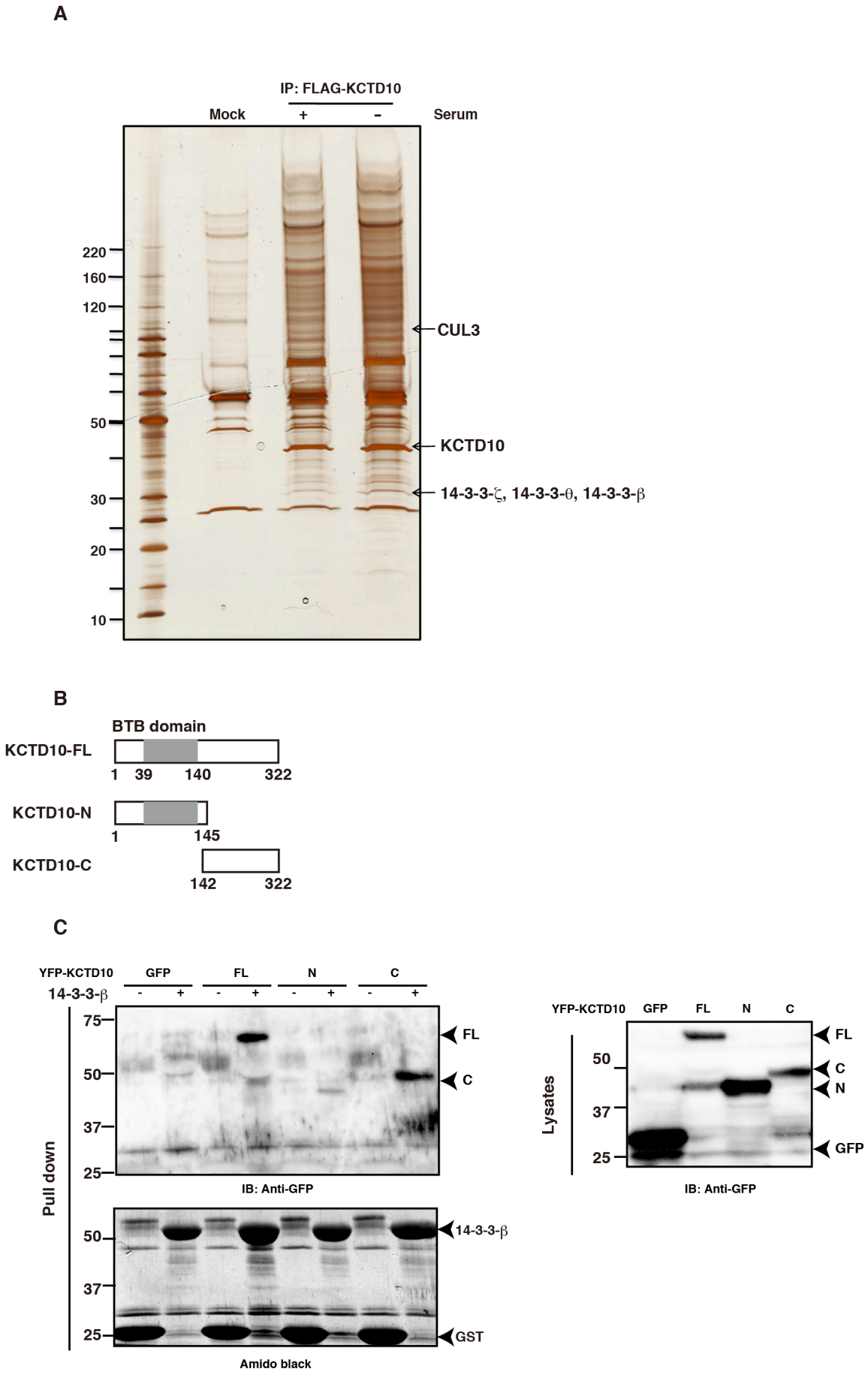
A
IP: FLAG-KCTD10
Mock
+
–
Serum
220
160
120
50
30
20
10
CUL3
KCTD10
14-3-3-ζ, 14-3-3-θ, 14-3-3-β
B
BTB domain
KCTD10-FL
1
39
140
322
KCTD10-N
1
145
KCTD10-C
142
322
C
YFP-KCTD10
GFP
FL
N
C
14-3-3-β
-
+
75
50
37
25
FL
C
Pull down
IB: Anti-GFP
50
37
25
14-3-3-β
GST
Amido black
YFP-KCTD10
GFP
FL
N
C
Lysates
50
37
25
FL
C
N
GFP
IB: Anti-GFP

Fig. 1

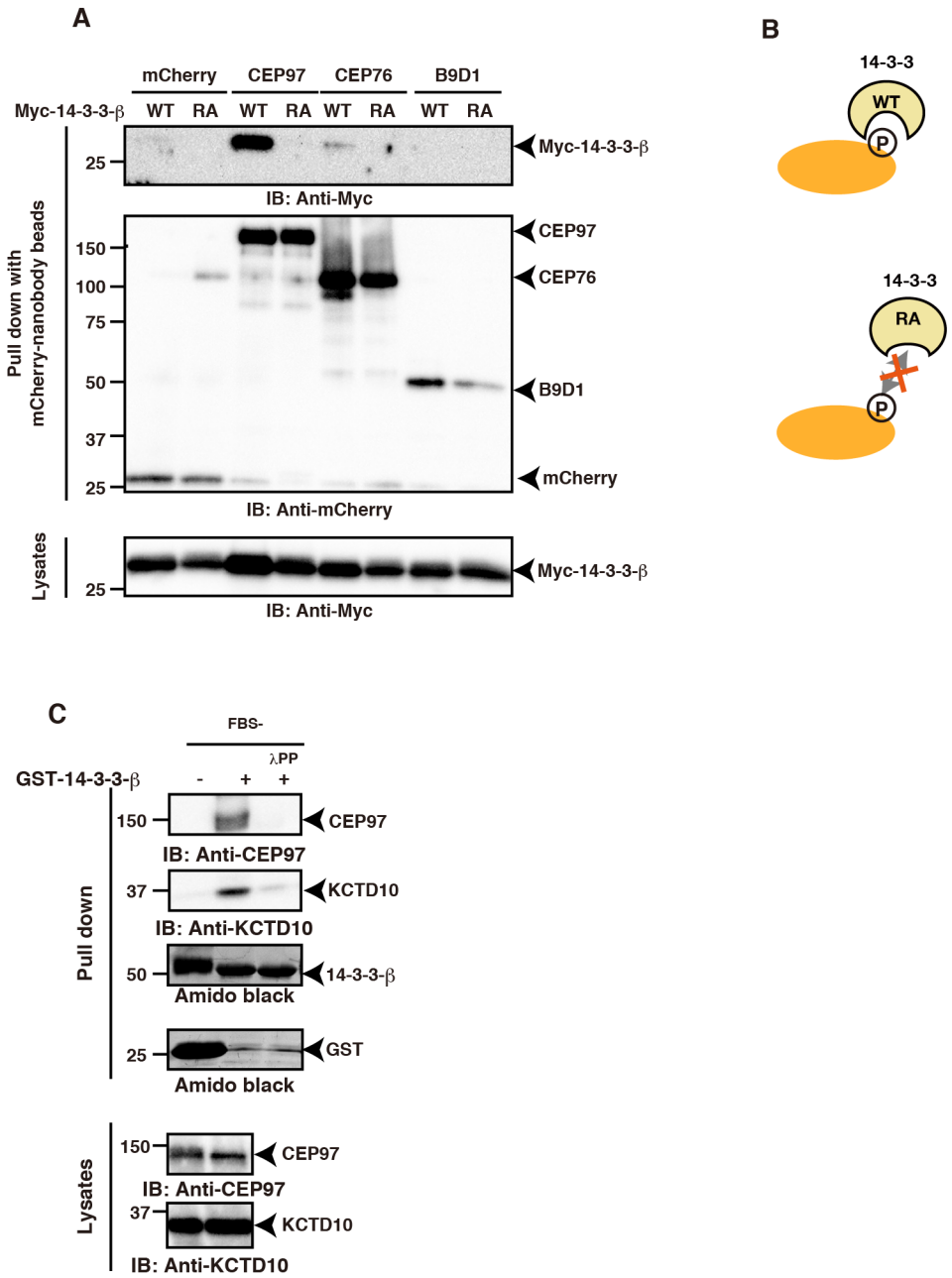
A
mCherry
CEP97
CEP76
B9D1
Myc-14-3-3-β
WT
RA
WT
RA
WT
RA
WT
RA
Myc-14-3-3-β
25
IB: Anti-Myc
Pull down with mCherry-nanobody beads
150
100
75
50
37
25
CEP97
CEP76
B9D1
mCherry
IB: Anti-mCherry
Lysates
25
Myc-14-3-3-β
IB: Anti-Myc
B
14-3-3
WT
P
14-3-3
RA
P
C
FBS-
λPP
GST-14-3-3-β
-
+
+
150
CEP97
IB: Anti-CEP97
37
KCTD10
IB: Anti-KCTD10
Pull down
50
14-3-3-β
Amido black
25
GST
Amido black
Lysates
150
CEP97
IB: Anti-CEP97
37
KCTD10
IB: Anti-KCTD10

Fig. 2

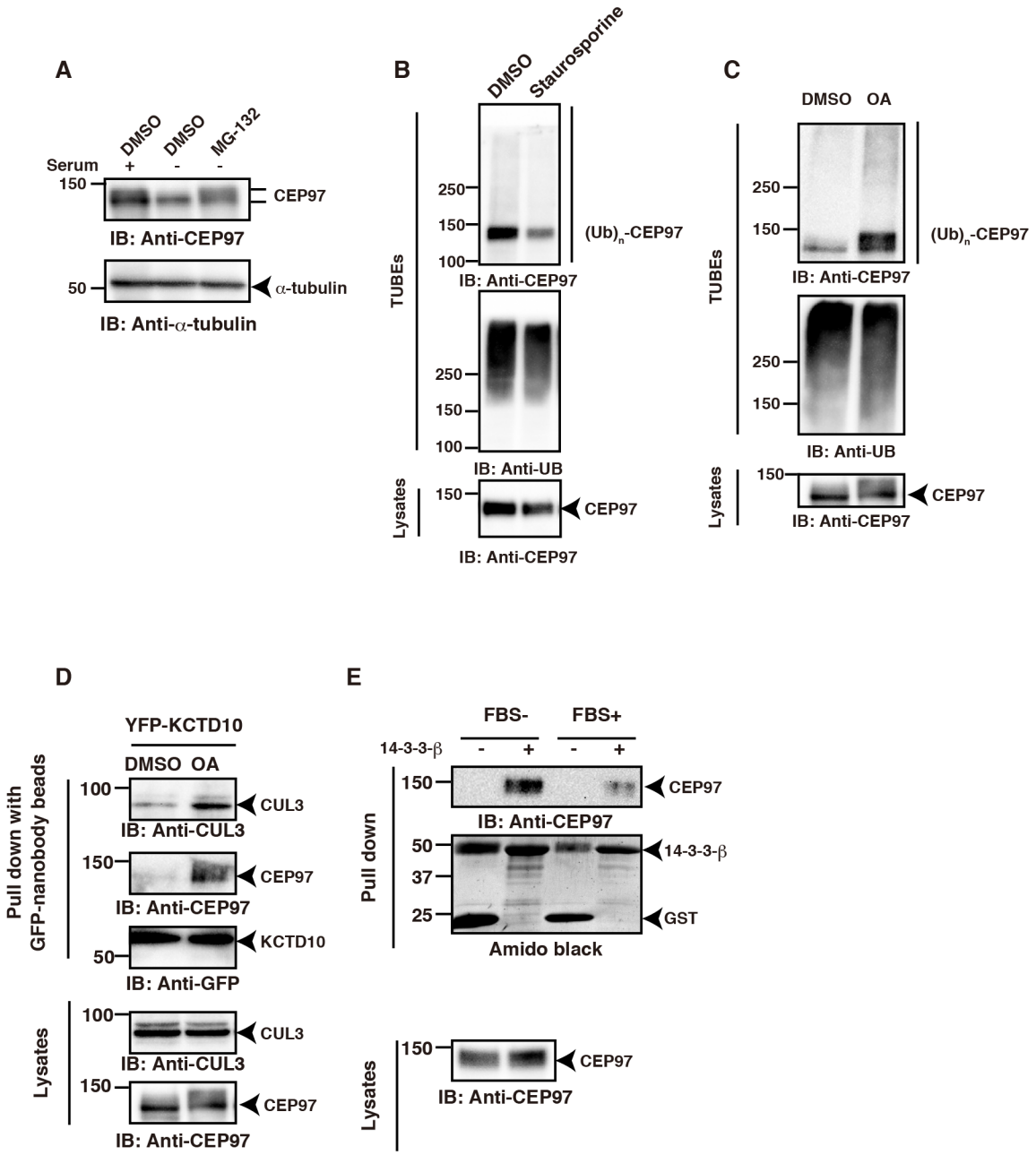
A
DMSO
DMSO
MG-132
Serum
+
-
-
150
CEP97
IB: Anti-CEP97
50
α-tubulin
IB: Anti-α-tubulin
B
DMSO
Staurosporine
TUBEs
250
150
100
(Ub)n-CEP97
IB: Anti-CEP97
250
150
100
IB: Anti-UB
Lysates
150
CEP97
IB: Anti-CEP97
C
DMSO
OA
TUBEs
250
150
(Ub)n-CEP97
IB: Anti-CEP97
250
150
IB: Anti-UB
Lysates
150
CEP97
IB: Anti-CEP97
D
YFP-KCTD10
DMSO
OA
Pull down with GFP-nanobody beads
100
CUL3
IB: Anti-CUL3
150
CEP97
IB: Anti-CEP97
50
KCTD10
IB: Anti-GFP
Lysates
100
CUL3
IB: Anti-CUL3
150
CEP97
IB: Anti-CEP97
E
FBS-
FBS+
14-3-3-β
-
+
-
+
Pull down
150
CEP97
IB: Anti-CEP97
50
37
25
14-3-3-β
GST
Amido black
Lysates
150
CEP97
IB: Anti-CEP97

Fig. 3

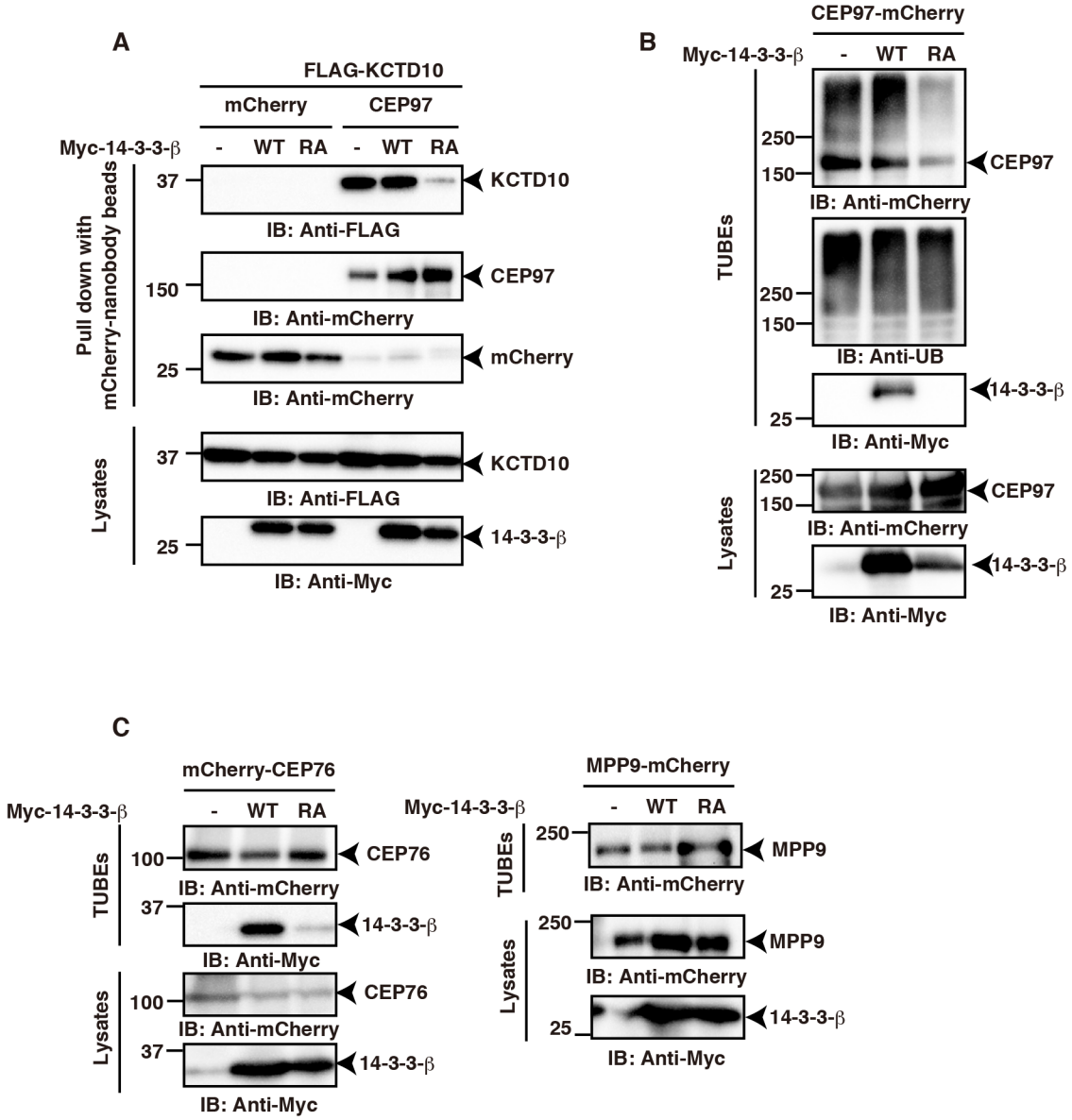
A
FLAG-KCTD10
mCherry
CEP97
Myc-14-3-3-β
-
WT
RA
-
WT
RA
Pull down with mCherry-nanobody beads
37
KCTD10
IB: Anti-FLAG
150
CEP97
IB: Anti-mCherry
25
mCherry
IB: Anti-mCherry
Lysates
37
KCTD10
IB: Anti-FLAG
25
14-3-3-β
IB: Anti-Myc
B
CEP97-mCherry
Myc-14-3-3-β
-
WT
RA
TUBEs
250
150
CEP97
IB: Anti-mCherry
250
150
IB: Anti-UB
25
14-3-3-β
IB: Anti-Myc
Lysates
250
150
CEP97
IB: Anti-mCherry
25
14-3-3-β
IB: Anti-Myc
C
mCherry-CEP76
Myc-14-3-3-β
-
WT
RA
TUBEs
100
CEP76
IB: Anti-mCherry
37
14-3-3-β
IB: Anti-Myc
Lysates
100
CEP76
IB: Anti-mCherry
37
14-3-3-β
IB: Anti-Myc
MPP9-mCherry
Myc-14-3-3-β
-
WT
RA
TUBEs
250
MPP9
IB: Anti-mCherry
Lysates
250
MPP9
IB: Anti-mCherry
25
14-3-3-β
IB: Anti-Myc

Fig. 4

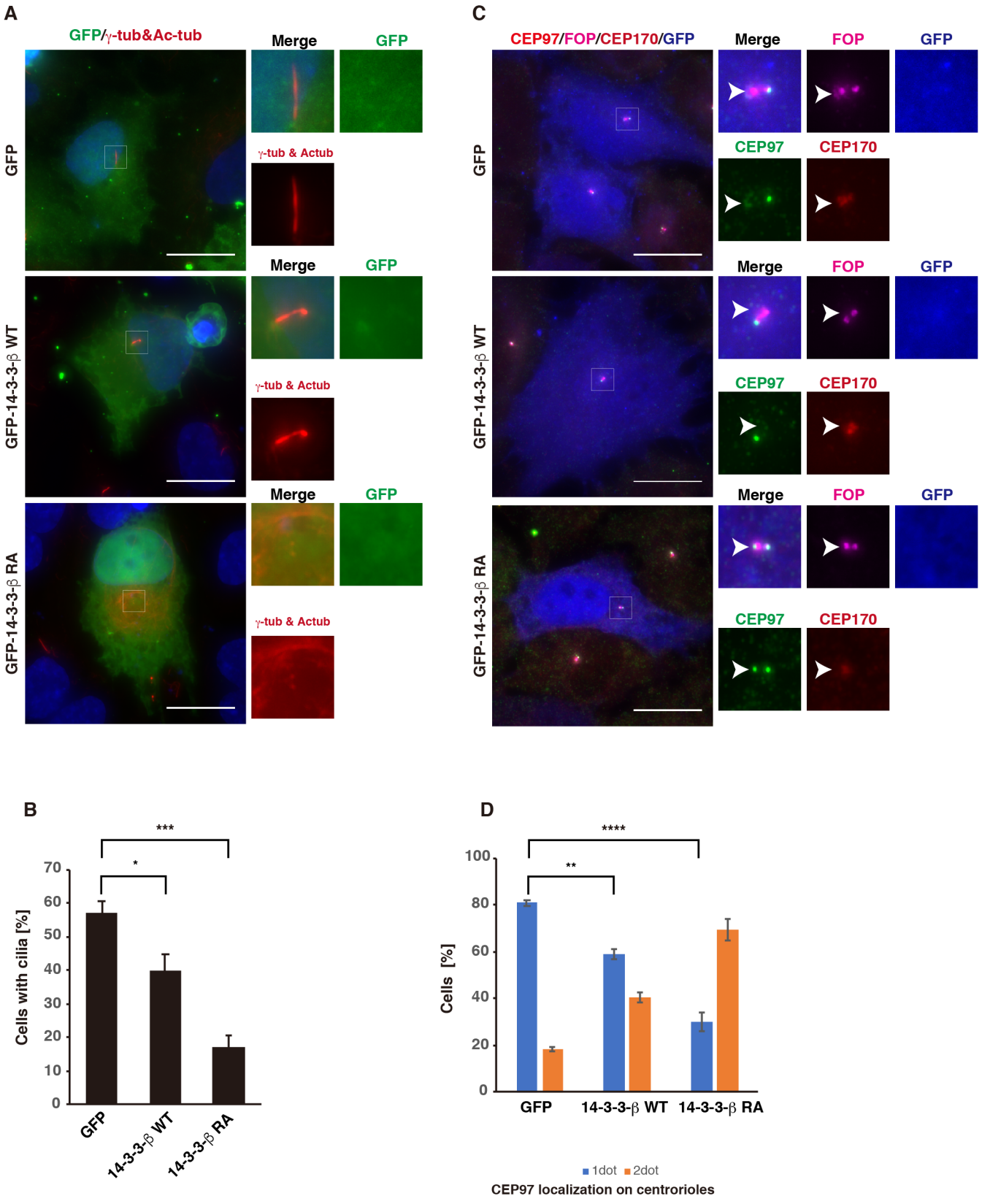
A
GFP/γ-tub&Ac-tub
Merge
GFP
γ-tub & Actub
GFP
GFP-14-3-3-β WT
GFP-14-3-3-β RA
C
CEP97/FOP/CEP170/GFP
Merge
FOP
GFP
CEP97
CEP170
B
Cells with cilia [%]
GFP
14-3-3-β WT
14-3-3-β RA
D
Cells [%]
1dot
2dot
CEP97 localization on centrorioles

Fig. 5

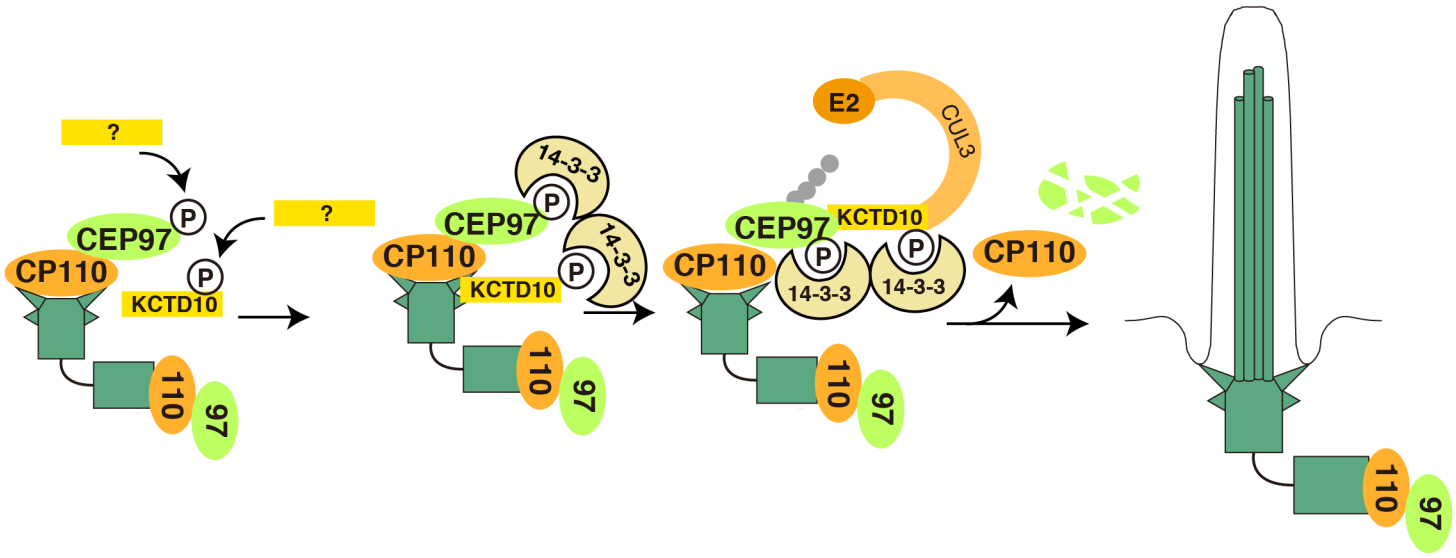
?
P
CEP97
CP110
KCTD10
?
P
110
97
14-3-3
P
CEP97
CP110
KCTD10
14-3-3
P
110
97
E2
CUL3
CEP97
KCTD10
P
P
CP110
14-3-3
14-3-3
110
97
CP110
110
97

Fig. 6

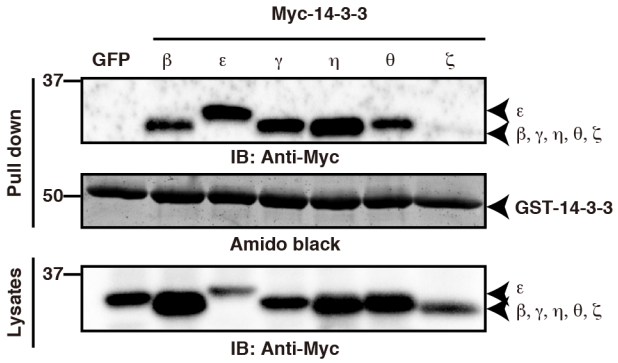
Myc-14-3-3
GFP
β
ε
γ
η
θ
ζ
37
Pull down
ε
β, γ, η, θ, ζ
IB: Anti-Myc
50
GST-14-3-3
Amido black
37
Lysates
ε
β, γ, η, θ, ζ
IB: Anti-Myc

Fig. S1

Acknowledgements

The research presented in this study was carried out in Mizuno laboratory and Ohashi laboratory, Tohoku University, under supervision of Prof. K. Mizuno and Prof. K. Ohashi. Their continuous encouragements and elaborate guidance are greatly appreciated. I wish to thank Dr. S. Kanno (Tohoku University) for analysis of mass spectrometry and insightful suggestions. I am very grateful to Dr. T. Nagai (Fukushima Medical University) and Dr. S. Chiba (Osaka City University) for their technical advice, insightful suggestions, and valuable discussions of my thesis. I wish to thank Dr. S. Ohata (Musashino University) for insightful suggestions. I also thank Dr. K. Yamashita (Tohoku University) for technical suggestion. I want to thank members at the Mizuno laboratory and Ohashi laboratory for their advice and support. Finally, I would like to thank my family for their support.